

Krylov's State Complexity and Information Geometry in Qubit Dynamics

Carlo Cafaro¹, Emma Clements², Vishnu Vardhan Anuboyina²

¹ Department of Nanoscale Science and Engineering,

University at Albany-SUNY, Albany, NY 12222, USA and

² Department of Physics, University at Albany-SUNY, Albany, NY 12222, USA

We compare Krylov's state complexity with an information-geometric (IG) measure of complexity for the quantum evolution of two-level systems. Focusing on qubit dynamics on the Bloch sphere, we analyze evolutions generated by stationary and nonstationary Hamiltonians, corresponding to geodesic and nongeodesic trajectories. We formulate Krylov complexity in geometric terms, both instantaneously and in a time-averaged sense, and contrast it with an IG complexity of quantum evolutions characterized in terms of efficiency and curvature. We show that the two measures reflect fundamentally different aspects of quantum dynamics: Krylov's state complexity quantifies the directional spread of the evolving state relative to the initial state, whereas the IG complexity captures the effective volume explored along the trajectory on the Bloch sphere. This geometric distinction explains their inequivalent behavior and highlights the complementary nature of state-based and information-geometric notions of complexity in quantum systems.

PACS numbers: Complexity (89.70.Eg), Entropy (89.70.Cf), Probability Theory (02.50.Cw), Quantum Computation (03.67.Lx), Quantum Information (03.67.Ac), Riemannian Geometry (02.40.Ky).

I. INTRODUCTION

In the domain of quantum physics, various concepts of complexity are present [1, 2]. For instance, one might refer to the complexity linked to a quantum state, the complexity intrinsic to a quantum circuit, or the complexity associated with an operator. Although these measures of complexity possess unique characteristics, they are united by a common principle: the complexity of a composite entity generally increases in relation to the number of fundamental components necessary for its construction. Depending on the context, this relationship can frequently be expressed through geometrically intuitive concepts such as *lengths*, *spread*, and *volumes*.

In the area of theoretical computer science, Kolmogorov proposed in Ref. [3] that the complexity of a sequence can be measured by the length of the shortest Turing machine program that can generate it. Furthermore, in the field of information theory, Rissanen indicated in Refs. [4, 5] that the average minimal code length of a collection of messages acts as a measure of the complexity of that set. Quantum circuits are composed of quantum gates that function on quantum states. Specifically, circuit complexity pertains to the minimum number of primitive gates necessary to create a circuit that executes a transformation on a designated quantum state [6, 7]. The geometric characterization of circuit complexity was introduced by Nielsen and his associates in Refs. [8–10]. Within this geometric framework, the circuit complexity related to a unitary operator U is fundamentally continuous and corresponds to the length of the shortest geodesic that connects the identity operator to U within the unitary group. The lengths of these geodesic paths provide a lower bound for the minimum number of quantum gates needed to construct the unitary operator U .

In gravity and quantum field theory, Krylov's state complexity [11] characterizes complexity as the least extent of the wavefunction's spread within the Hilbert space, whereas Krylov's operator complexity [12] seeks to measure the rate at which operators disperse in the entirety of operator space during their evolution. To establish a cohesive framework for articulating the complexities of Krylov's operator and state, we recommend consulting Ref. [13]. The initial attempts to understand Krylov's complexity from a geometric perspective were conducted in Refs. [14, 15]. In Ref. [15], for example, during the examination of instances of irrational two-dimensional conformal field theories, it was demonstrated that Krylov's operator complexity is proportional to the volume in the information geometry defined by the Fubini-Study metric, which serves as a distance measure between pure quantum states. In Ref. [16], it was demonstrated that the time average of Krylov complexity related to state evolution can be represented as a trace of a particular matrix. This matrix also specifies an upper limit on Nielsen complexity, which is fundamentally geometric as it is associated with geodesic flows on curved manifolds, accompanied by a specially designed penalty schedule tailored to the Krylov basis. In Ref. [17], it was observed that the Krylov complexities among three states do not adhere to the triangle inequality, thus rendering them unsuitable as a measure of distance between these states: there exists no metric for which Krylov complexity represents the length of the shortest path to the target state or operator. This is explicitly illustrated in the simplest case of a single qubit, as well as in a general context. In Ref. [18], the authors illustrated in the context of a single qubit that the square root of Krylov's state complexity quantifies the distance between states that have evolved over time. They achieved this by explicitly constructing a corresponding parameter space onto which the states within the Hilbert space are mapped.

In Refs. [19, 20], we introduced a metric for assessing the complexity of quantum evolution, defined by the ratio of

the difference between accessible and accessed Bloch-sphere volumes during the transition from the initial to the final state, relative to the accessible volume for the specified quantum evolution. Specifically, we examined the complexity associated with both time-optimal and time sub-optimal quantum Hamiltonian evolutions that connect arbitrary source and target states on the Bloch sphere, utilizing the Fubini-Study metric. This analysis was conducted in several stages. Initially, we characterized each unitary Schrödinger quantum evolution through parameters such as path length, geodesic efficiency [21], speed efficiency [22], and the curvature coefficient [23–28] of the corresponding dynamical trajectory that links the source state to the target state [29, 30]. Subsequently, we began with a classical probabilistic framework where the concept of information geometric complexity is applicable to describe the complexity of entropic motion on curved statistical manifolds, which underpin the physics of systems when only partial information is available [31–34]. We then transitioned to a deterministic quantum framework. In this setting, after establishing a definition for the complexity of quantum evolution, we introduced the concept of quantum complexity length scale. We particularly emphasized the physical relevance of both quantities concerning the accessed (i.e., partial) and accessible (i.e., total) parametric volumes of the regions on the Bloch sphere that delineate the quantum mechanical evolution from the source to the target states. Finally, after computing the complexity measure and the complexity length scale for each of the two quantum evolutions, we compared the behavior of our measures with that of path length, geodesic efficiency, speed efficiency, and curvature coefficient [29, 30]. Our findings indicated that, generally, efficient quantum evolutions exhibit lower complexity than their inefficient counterparts. Nonetheless, we also noted that complexity encompasses more than mere length. Indeed, elongated paths that are adequately curved can demonstrate a behavior that is simpler than that of shorter paths with a lower curvature coefficient.

Driven by the quest for a cohesive geometrical understanding of complexity measures, we concentrate on Krylov's state complexity alongside our quantum IG measure of complexity. This approach aims to provide insights into their similarities and differences through a comparative analysis that utilizes explicit illustrative examples. Some of the inquiries we aim to explore in this paper include:

- [i] In the context of two-level quantum systems, can we articulate Krylov's state complexity using vectors that possess a distinct geometric significance?
- [ii] Is there a connection between Krylov's state complexity and the notions of distance among Bloch vectors, or the Fubini-Study finite volume element assessed through the spherical angles that parameterize qubit states on the Bloch sphere?
- [iii] What unique features of quantum evolution are represented by Krylov's state complexity and our quantum IG complexity measure when examining both geodesic and non-geodesic evolutions governed by stationary or non-stationary Hamiltonian dynamics?
- [iv] Do longer trajectories that link the same initial and final states on the Bloch sphere inherently exhibit higher levels of Krylov's state complexity? How do relative phases in quantum states influence the behavior of Krylov's state complexity and our quantum IG complexity measure?

The significance of addressing these inquiries is twofold. Firstly, similar to other geometric quantifiers of quantum evolutions, such as geodesic efficiency, speed efficiency, and the curvature coefficient of quantum evolutions, it enables the expression of Krylov's state complexity in terms of straightforward real-valued three-dimensional vectors that have a clear geometric interpretation. This facilitates a more cohesive understanding of quantum evolutions from a geometric perspective, utilizing quantifiers that can all be represented as simple real-valued vectors with an easily comprehensible geometric meaning. Secondly, it provides an opportunity to acquire new physical insights regarding the complexity of quantum evolutions by contrasting two distinct measures, each highlighting specific characteristics of quantum evolutions, both of which are related to common concepts such as length, spread, and volume.

The remainder of this paper is structured as follows. In Section II, we provide a concise overview of the physics pertaining to two-level systems, highlighting the functional forms of the unitary time-propagators across various “magnetic” field configurations. In this context, we present the fundamental elements of the concepts of geodesic efficiency and the curvature coefficient associated with quantum evolutions. Section III introduces the essential characteristics of Krylov's state complexity alongside our quantum IG complexity measure for quantum evolutions. In Section IV, we reformulate both the instantaneous and time-averaged Krylov state complexity for stationary and nonstationary Hamiltonian evolutions, representing them through two real-valued vectors that possess clear geometric significance. In the stationary scenario, these vectors correspond to the Bloch vector of the initial state and the unit vector that defines the magnetic field vector incorporated into the Hamiltonian. Conversely, in the nonstationary scenario, the two vectors represent the Bloch vector of the initial state and that of the time-evolved state at a subsequent time t . These geometrically significant expressions of Krylov's state complexity are employed not only to explore configurations that result in maximal and sub-maximal complexity levels but also to examine

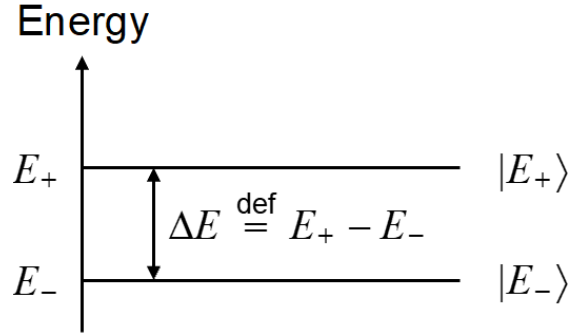


FIG. 1: Sketch of an energy level diagram for a two-level system. The Hamiltonian H of the system has a spectral decomposition given by $H = E_- |E_- \rangle \langle E_-| + E_+ |E_+ \rangle \langle E_+|$, with energy gap $\Delta E \stackrel{\text{def}}{=} E_+ - E_- \geq 0$. In general, $|E_+ \rangle = |e\rangle = |\uparrow\rangle$ denotes the excited state or spin up state (maximum eigenvalue), while $|E_- \rangle = |g\rangle = |\downarrow\rangle$ denotes the ground state or spin down state (minimum eigenvalue).

the distinctions observed when comparing stationary and nonstationary qubit dynamics. In Section V, we conduct a comparative analysis of these two complexity measures by explicitly examining both geodesic and nongeodesic evolutions characterized by time-independent Hamiltonians. In Section VI, we follow a similar approach to Section V, substituting stationary Hamiltonian evolutions with nonstationary ones. Our concluding remarks are presented in Section VII, while additional technical details can be found in the appendices.

II. EFFICIENCY AND CURVATURE IN QUBIT DYNAMICS

In this section, considering their application in the upcoming sections, we introduce the notions of geodesic efficiency and curvature coefficient pertaining to quantum evolutions. These notions can be articulated for any arbitrary finite-dimensional quantum systems in a pure state. Nevertheless, our focus here is on two-dimensional systems and their geometric representations.

A. Two-level systems

In this subsection, we present a brief summary of the physics related to two-level systems, emphasizing the functional representations of the unitary time-propagators under different “magnetic” field arrangements. Two-level systems are significant for at least three reasons. Firstly, they represent the simplest systems in quantum mechanics as they encompass a two-dimensional Hilbert space. Secondly, they are quite prevalent in nature and are extensively utilized in atomic physics. Thirdly, a two-level system is synonymous with the qubit, which serves as the fundamental building block of the rapidly advancing field of quantum information and computation. In Fig. 1, we display an energy level diagram for a two-level system.

Typical instances of two-level systems include a spin-1/2 particle (such as an electron) in a magnetic field and a two-level atom. The Hamiltonian for the former system is defined by the term $-\vec{\mu} \cdot \mathbf{B}(t)$ (Zeeman effect), where $\vec{\mu} = \frac{e}{mc} \mathbf{s} = \frac{e\hbar}{2mc} \boldsymbol{\sigma} = \mu_B \boldsymbol{\sigma}$ represents the magnetic moment operator of the electron in cgs-units, μ_B signifies the Bohr magneton, and $\mathbf{B}(t)$ denotes the time-dependent magnetic field vector. The Hamiltonian for the latter system is characterized by the term $-\mathbf{d} \cdot \mathbf{E}(t)$ (Stark effect), where $\mathbf{d} \stackrel{\text{def}}{=} e\mathbf{r}$ represents the electric dipole moment operator of the electron, and $\mathbf{E}(t)$ signifies the external electric field. To elaborate on \mathbf{d} , let us consider $|g\rangle$ and $|e\rangle$ as the ground and excited states, respectively. Thus, we can express \mathbf{d} as $\mathbf{d} = e\mathbf{r} = \mathbf{d}_{eg} |e\rangle \langle g| + \mathbf{d}_{ge} |g\rangle \langle e|$, where $\mathbf{d}_{eg} \stackrel{\text{def}}{=} \langle e | \mathbf{d} | g \rangle$ and $\mathbf{d}_{ge} \stackrel{\text{def}}{=} \langle g | \mathbf{d} | e \rangle$. In the case of a hydrogen atom, the transition from $|g\rangle$ and $|e\rangle$ is defined by the transition between the $1s$ state (with quantum number $l = 0$) and the $2p$ state (with $l = 1$). From the expression of \mathbf{d} , it is observed that the off-diagonal terms facilitate the transitions, whereas the diagonal terms disappear due to parity. In fact, the dipole operator is odd with respect to parity (i.e., $\mathbf{d} \xrightarrow{\text{parity}} -\mathbf{d}$), which necessitates that dipole transitions occur

between states of opposite parity. It is evident that a two-level atom is fundamentally analogous to a spin-1/2 particle subjected to a magnetic field.

The fundamental dynamical equations derived from Schrödinger's equation that dictate the evolution of the variables of a two-level atom are essentially identical to those applicable to spins. In a time-independent framework, the most comprehensive (traceless and stationary) Hamiltonian model of a two-level system can be reformulated as

$$H = \frac{\hbar}{2} \begin{pmatrix} \Delta & \Omega^* \\ \Omega & -\Delta \end{pmatrix} = \frac{\hbar}{2} \begin{pmatrix} \Delta & \Omega_x - i\Omega_y \\ \Omega_x + i\Omega_y & -\Delta \end{pmatrix}. \quad (1)$$

In a spin-1/2 system, Δ represents the Zeeman splitting, whereas Ω indicates the magnetic field applied in the xy -plane. Conversely, in a laser-driven two-level atom, Δ signifies the difference between the laser frequency and the transition frequencies, while Ω is proportional to the product of the atomic dipole moment and the amplitude of the electric field.

In the rest of the paper, we assume to deal with an Hamiltonian which can be generally non-traceless and nonstationary given by

$$H(t) \stackrel{\text{def}}{=} h_0(t) \mathbf{1} + \mathbf{h}(t) \cdot \boldsymbol{\sigma}, \quad (2)$$

with $\mathbf{h}(t) \stackrel{\text{def}}{=} (h_x(t), h_y(t), h_z(t))$ being improperly called here a "magnetic" field vector (since, from a physical dimension standpoint, it is measures in joules in MKSA units) and $\boldsymbol{\sigma} \stackrel{\text{def}}{=} (\sigma_x, \sigma_y, \sigma_z)$ denoting the three Pauli spin operators. The quantity " $\mathbf{1}$ " in Eq. (2) is the identity operator acting on the single-qubit Hilbert space.

We note that when the Hamiltonian remains constant over time, the unitary time propagator is expressed as $U(t) \stackrel{\text{def}}{=} e^{-\frac{i}{\hbar} H t}$. From a physics perspective, this scenario would represent a spin-magnetic moment interacting with a static magnetic field. In cases where the Hamiltonian varies with time but the Hamiltonians at different instances commute, we have $U(t) \stackrel{\text{def}}{=} \exp(-\frac{i}{\hbar} \int_0^t H(t') dt')$. Physically, this situation corresponds to a spin-magnetic moment experiencing a magnetic field that changes in strength over time while maintaining a constant direction. Lastly, when the Hamiltonian is time-dependent and the Hamiltonians at different times do not commute, we encounter

$$U(t) \stackrel{\text{def}}{=} \mathcal{T} \exp\left(-\frac{i}{\hbar} \int_0^t H(t') dt'\right) = \mathbf{1} + \sum_{n=1}^{\infty} \left(\frac{-i}{\hbar}\right)^n \int_0^t dt_1 \int_0^{t_1} dt_2 \dots \int_0^{t_{n-1}} dt_n H(t_1) H(t_2) \dots H(t_n), \quad (3)$$

with $0 \leq t_n \leq t_{n-1} \leq \dots \leq t_2 \leq t_1 \leq t$. In Eq. (3), the symbol " \mathcal{T} " represents the time-ordering operator, and the series expansion is referred to as the Dyson series expansion [35]. From a physics perspective, this unitary time propagator appears when examining a spin-magnetic moment that is influenced by a magnetic field whose direction varies over time (while its magnitude may either fluctuate or remain constant). In this series expansion in Eq. (3), $\mathbf{1}$ is the zeroth order term, $(-i/\hbar) \int_0^t dt_1 H(t_1)$ is the first order term, and $(-i/\hbar)^2 \int_0^t dt_1 \int_0^{t_1} dt_2 H(t_1) H(t_2)$ is the second order term. We observe that when the Hamiltonian remains constant over time, the Dyson series in Eq. (3) simplifies precisely to the well-known exponential representation of the time-evolution operator

$$U(t) = \mathbf{1} + \sum_{n=1}^{\infty} \left(\frac{-i}{\hbar}\right)^n H^n \frac{t^n}{n!} = \sum_{n=0}^{\infty} \left(\frac{-i}{\hbar}\right)^n H^n \frac{t^n}{n!} = e^{-\frac{i}{\hbar} H t}. \quad (4)$$

This occurs due to the commutation of all Hamiltonians at various times, rendering time ordering unnecessary and transforming the Dyson expansion into a standard exponential series. Furthermore, although the Dyson integral covers one ordering of time, if all Hamiltonians commute, all time orderings give the same contribution, and there are $n!$ of them. Therefore, when $[H(t_i), H(t_j)] = 0$ for any t_i and t_j , we have

$$U(t) = \mathbf{1} + \sum_{n=1}^{\infty} \left(\frac{-i}{\hbar}\right)^n \frac{1}{n!} \left(\int_0^t H(t') dt'\right)^n = \sum_{n=0}^{\infty} \left(\frac{-i}{\hbar}\right)^n \frac{1}{n!} \left(\int_0^t H(t') dt'\right)^n = e^{-\frac{i}{\hbar} \int_0^t H(t') dt'}. \quad (5)$$

In Fig. 2, we illustrate a variety of magnetic field vector configurations $\mathbf{B}(t)$ with $\mathbf{h}(t) \propto \mathbf{B}(t)$ that ultimately lead to one of the time propagators as presented in Eqs. (3) (i. e., $\mathbf{B} = B(t) \hat{B}(t)$ or $\mathbf{B} = B_0 \hat{B}(t)$), (4) (i. e., $\mathbf{B} = B_0 \hat{B}_0$), and (5) (i. e., $\mathbf{B} = B(t) \hat{B}_0$). In this paper, we examine quantum-mechanical evolutions defined by all magnetic field configurations presented in (a), (b), (c), and (d) of Fig. 2. For additional information regarding two-level systems, we direct the reader to Refs. [36, 37].

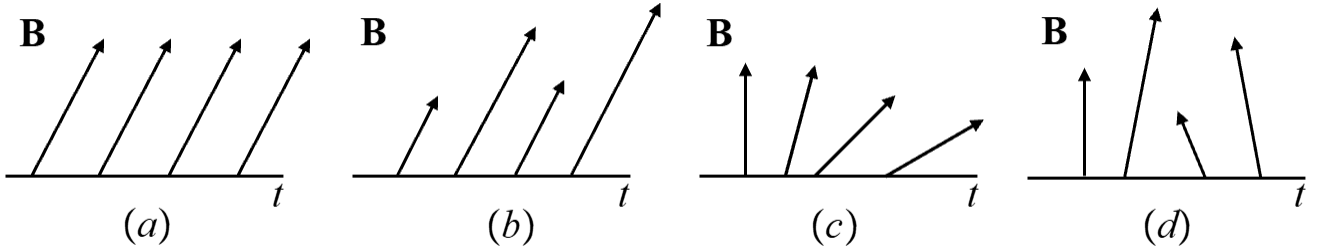


FIG. 2: Sketch of a variety of magnetic field vector configurations. In (a), $\mathbf{B} \stackrel{\text{def}}{=} B_0 \hat{B}_0$. In (b), $\mathbf{B} \stackrel{\text{def}}{=} B(t) \hat{B}_0$. In (c), $\mathbf{B} \stackrel{\text{def}}{=} B_0 \hat{B}(t)$. Finally, in (d), $\mathbf{B} \stackrel{\text{def}}{=} B(t) \hat{B}(t)$. We note that \mathbf{B} is the magnetic field vector, B_0 denotes a constant intensity, and \hat{B}_0 is a constant unit vector.

B. Efficiency and curvature

Concentrating on the dynamics of qubits, we will now outline the fundamental aspects of geodesic efficiency and the curvature coefficient pertaining to quantum evolutions limited to two-level systems.

1. Geodesic efficiency

The concept of geodesic efficiency in quantum evolution was first proposed by Anandan and Aharonov in Ref. [21]. Consider the evolution of a state vector $|\psi(t)\rangle$ governed by the time-dependent Schrödinger equation, $i\hbar\partial_t|\psi(t)\rangle = H(t)|\psi(t)\rangle$, within the interval $t_A \leq t \leq t_B$. Consequently, the geodesic efficiency η_{GE} for this quantum evolution is a time-independent (global) scalar quantity, constrained by $0 \leq \eta_{\text{GE}} \leq 1$, as defined in [21]

$$\eta_{\text{GE}} \stackrel{\text{def}}{=} \frac{s_0}{s} = 1 - \frac{\Delta s}{s} = \frac{2 \arccos [\langle A | B \rangle]}{2 \int_{t_A}^{t_B} \frac{\Delta E(t)}{\hbar} dt}, \quad (6)$$

with $\Delta s \stackrel{\text{def}}{=} s - s_0$. The term s_0 represents the distance along the shortest geodesic path connecting the initial $|A\rangle \stackrel{\text{def}}{=} |\psi(t_A)\rangle$ and final $|B\rangle \stackrel{\text{def}}{=} |\psi(t_B)\rangle$ states within the complex projective Hilbert space. Furthermore, the variable s in Eq. (6) signifies the distance along the dynamical trajectory $\gamma(t) : t \mapsto |\psi(t)\rangle$ that corresponds to the evolution of the state vector $|\psi(t)\rangle$ for $t_A \leq t \leq t_B$. It is evident that a geodesic quantum evolution characterized by $\gamma(t) = \gamma_{\text{geodesic}}(t)$ is determined by the equation $\eta_{\text{GE}}^{(\gamma_{\text{geodesic}})} = 1$. Additionally, we observe that by setting $H(t) \stackrel{\text{def}}{=} h_0(t) \mathbf{1} + \mathbf{h}(t) \cdot \boldsymbol{\sigma}$ and $\rho(t) \stackrel{\text{def}}{=} (\mathbf{1} + \mathbf{a}(t) \cdot \boldsymbol{\sigma})/2$ with $t_A \leq t \leq t_B$, the energy uncertainty $\Delta E(t) \stackrel{\text{def}}{=} \sqrt{\text{tr}(\rho H^2) - [\text{tr}(\rho H)]^2}$ simplifies to $\Delta E(t) = \sqrt{\mathbf{h}^2 - [\mathbf{a}(t) \cdot \mathbf{h}]^2}$. Ultimately, the geodesic efficiency expressed in Eq. (6) can be reformulated as

$$\eta_{\text{GE}} = \frac{2 \arccos \left(\sqrt{\frac{1+\mathbf{a} \cdot \mathbf{b}}{2}} \right)}{\int_{t_A}^{t_B} \frac{2}{\hbar} \sqrt{\mathbf{h}^2 - [\mathbf{a}(t) \cdot \mathbf{h}]^2} dt}, \quad (7)$$

where $\mathbf{a}(t_A) \stackrel{\text{def}}{=} \mathbf{a}$ and $\mathbf{a}(t_B) = \mathbf{b}$ in Eq. (7). Interestingly, for $H(t) \stackrel{\text{def}}{=} \mathbf{h}(t) \cdot \boldsymbol{\sigma}$ and by $\mathbf{h} \stackrel{\text{def}}{=} [\mathbf{h} \cdot \mathbf{a}] \mathbf{a} + [\mathbf{h} - (\mathbf{h} \cdot \mathbf{a}) \mathbf{a}] = \mathbf{h}_{\parallel} + \mathbf{h}_{\perp}$, where $\mathbf{a} = \mathbf{a}(t)$ in the decomposition of \mathbf{h} , η_{GE} in Eq. (7) reduces to

$$\eta_{\text{GE}} = \frac{\arccos \left(\sqrt{\frac{1+\mathbf{a} \cdot \mathbf{b}}{2}} \right)}{\int_{t_A}^{t_B} h_{\perp}(t) dt}. \quad (8)$$

Consequently, from Eq. (8), it is evident that η_{GE} is solely dependent on the initial Bloch vector \mathbf{a} , the final Bloch vector \mathbf{b} , and the magnitude $h_{\perp}(t) \stackrel{\text{def}}{=} \|\mathbf{h}_{\perp}\|$ of the vector component of the magnetic field that is perpendicular to the time-dependent Bloch vector $\mathbf{a}(t)$. For further information regarding the concept of geodesic efficiency, we recommend consulting Refs. [21, 29, 30].

2. Curvature

In the realm of quantum-mechanical processes, the curvature coefficient, which varies with time, is defined by the square of the magnitude of the covariant derivative of the tangent vector associated with the time-evolving state vector [27, 28]. Specifically, this curvature coefficient quantifies the curvature of the quantum trajectory formed by a pure quantum state that is parallel-transported and evolves unitarily under a nonstationary Hamiltonian, which governs the Schrödinger evolution equation.

For two-level systems, the curvature coefficient κ_{AC}^2 in Refs.[27, 28] (with the subscript “AC” denoting Alsing and Cafaro) can be entirely articulated in terms of two distinct real three-dimensional vectors that possess clear geometric significance. These vectors are the Bloch vector $\mathbf{a}(t)$ and the magnetic field vector $\mathbf{h}(t)$. The former is derived from the density operator $\rho(t) = |\psi(t)\rangle\langle\psi(t)| \stackrel{\text{def}}{=} [\mathbf{1} + \mathbf{a}(t) \cdot \boldsymbol{\sigma}] / 2$, while the latter defines the nonstationary Hamiltonian $H(t) \stackrel{\text{def}}{=} \mathbf{h}(t) \cdot \boldsymbol{\sigma}$. Based on the comprehensive analysis presented in Ref. [28], we obtain

$$\kappa_{\text{AC}}^2(\mathbf{a}, \mathbf{h}) = 4 \frac{(\mathbf{a} \cdot \mathbf{h})^2}{\mathbf{h}^2 - (\mathbf{a} \cdot \mathbf{h})^2} + \frac{\left[\mathbf{h}^2 \dot{\mathbf{h}}^2 - (\mathbf{h} \cdot \dot{\mathbf{h}})^2 \right] - \left[(\mathbf{a} \cdot \dot{\mathbf{h}}) \mathbf{h} - (\mathbf{a} \cdot \mathbf{h}) \dot{\mathbf{h}} \right]^2}{\left[\mathbf{h}^2 - (\mathbf{a} \cdot \mathbf{h})^2 \right]^3} + 4 \frac{(\mathbf{a} \cdot \mathbf{h}) [\mathbf{a} \cdot (\mathbf{h} \times \dot{\mathbf{h}})]}{\left[\mathbf{h}^2 - (\mathbf{a} \cdot \mathbf{h})^2 \right]^2}, \quad (9)$$

where $\dot{\mathbf{h}} \stackrel{\text{def}}{=} d\mathbf{h}/dt$. The expression of κ_{AC}^2 in Eq. (9) is highly beneficial from a computational perspective for qubit systems and simultaneously provides a clear geometric interpretation of the curvature of quantum evolution in relation to the (normalized unitless) Bloch vector \mathbf{a} and the (generally unnormalized, $[\mathbf{h}]_{\text{MKSA}} = \text{joules} = \text{sec.}^{-1}$ when setting $\hbar = 1$) magnetic field vector \mathbf{h} . From Eq. (9), it is observed that for stationary Hamiltonian evolutions, κ_{AC}^2 simplifies to a time-independent quantity as indicated by [27]

$$\kappa_{\text{AC}}^2(\mathbf{a}, \mathbf{h}) = 4 \frac{(\mathbf{a} \cdot \mathbf{h})^2}{\mathbf{h}^2 - (\mathbf{a} \cdot \mathbf{h})^2}. \quad (10)$$

Evidently, when \mathbf{a} and \mathbf{h} are orthogonal in Eq. (10), the curvature coefficient $\kappa_{\text{AC}}^2(\mathbf{a}, \mathbf{h})$ becomes zero. To clarify, we emphasize that although $\mathbf{a} = \mathbf{a}(t)$ in Eq. (9), it is permissible to substitute $\mathbf{a}(t)$ with $\mathbf{a}(0)$ in Eq. (10). This is fundamentally because when the Hamiltonian H does not depend on time, $\langle\psi(t)|H|\psi(t)\rangle = \langle\psi(0)|H|\psi(0)\rangle$ (i.e., $\mathbf{a}(t) \cdot \mathbf{h} = \mathbf{a}(0) \cdot \mathbf{h}$). The conservation of $\langle H \rangle$ means that the projection of $\mathbf{a}(t)$ along \mathbf{h} is constant in time. For additional information regarding the concept of curvature in quantum mechanical evolutions, we recommend consulting Refs. [27–30].

After examining the essential elements of two-level systems and emphasizing the notions of efficiency and curvature, we are now ready to introduce the two types of complexity measures employed in our comparative analysis.

III. COMPLEXITY MEASURES

In this section, we present the fundamental features of Krylov’s state complexity in conjunction with our quantum IG complexity metric for quantum evolutions.

For completeness, we recall here that the geometry of the Bloch sphere endowed with the Fubini–Study metric can be interpreted as a form of quantum information geometry [38–40]. Indeed, when equipped with the Fubini–Study (FS) metric, the Bloch sphere constitutes a natural quantum information manifold for pure states. Moreover, the Fubini–Study metric is directly related to the quantum Fisher information metric, with $g_{\alpha\beta}^{\text{QFI}} = 4g_{\alpha\beta}^{\text{FS}}$ (for details, see Appendix A). Note that $1 \leq \alpha, \beta \leq \dim_{\mathbb{R}} \mathbb{C}\mathbb{P}^1 = 2$, where $\mathbb{C}\mathbb{P}^1$ is the complex Hilbert space for single-qubit pure states that is isomorphic to the Bloch sphere S^2 , with $S^2 \simeq \mathbb{C}\mathbb{P}^1$.

Following this series of comments, we are prepared to present Krylov’s state complexity.

A. Krylov’s state complexity

Let us examine a quantum-mechanical system that progresses under a stationary Hamiltonian H . We assume that the time evolution of a state $|\psi(t)\rangle$ is governed by the Schrödinger equation $i\hbar\partial_t|\psi(t)\rangle = H|\psi(t)\rangle$. Consequently, the solution to the evolution equation can be articulated as

$$|\psi(t)\rangle = e^{-\frac{i}{\hbar}Ht}|\psi(0)\rangle = \sum_{n=0}^{+\infty} \frac{(-it)^n}{\hbar^n n!} |\psi_n\rangle, \quad (11)$$

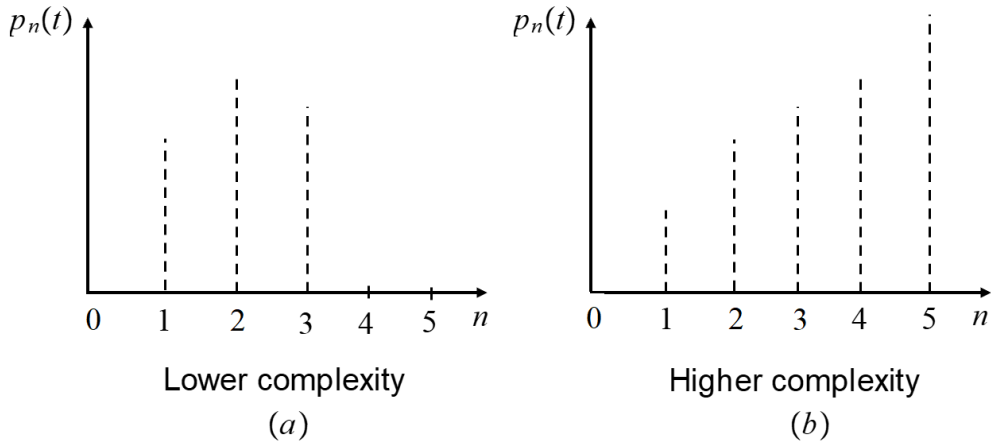


FIG. 3: Illustrations of low (a) and high (b) scenarios of Krylov state complexity $\mathcal{K}(t)$. In both (a) and (b), n represents the Krylov index, while the dashed vertical lines indicate the probabilities $p_n(t) \stackrel{\text{def}}{=} |\langle K_n | \psi(t) \rangle|^2$. The Krylov state complexity $\mathcal{K}(t)$ is defined as the average position $\langle n \rangle$ of this probability distribution $p_n(t)$ with $0 \leq p_n(t) \leq 1$ and $\sum_n p_n(t) = 1$. In scenario (a), the wavefunction exhibits minimal spreading, resulting in a slow increase in Krylov's state complexity. Generally, a low complexity scenario is characterized by a narrow distribution concentrated around $n = 0$. Conversely, in scenario (b), the state investigates numerous Krylov directions, leading to a rapid increase in Krylov's state complexity. Typically, a high energy scenario is marked by a wide distribution with its center significantly distant from $n = 0$.

with $|\psi_n\rangle \stackrel{\text{def}}{=} H^n |\psi(0)\rangle$. The Gram-Schmidt orthonormalization method applied to $\{|\psi_n\rangle\} = \{|\psi(0)\rangle, H|\psi(0)\rangle, H^2|\psi(0)\rangle, \dots\}$ results in an ordered, orthonormal basis $\{K_n\}$ for the segment of the Hilbert space that is investigated by the evolving state $|\psi(0)\rangle \equiv |K_0\rangle$. The Krylov basis $\{K_n\}$ may contain fewer elements than the dimension of the Hilbert space, contingent upon the dynamics and the selection of the initial state. The Krylov basis can be formally represented through the Lanczos recursive algorithm as [41],

$$\begin{cases} |A_{n+1}\rangle = (H - a_n) |K_n\rangle - b_n |K_{n-1}\rangle \\ |K_n\rangle = b_n^{-1} |A_n\rangle \end{cases}, \quad (12)$$

where $b_n \stackrel{\text{def}}{=} \langle A_n | A_n \rangle$, $b_0 \stackrel{\text{def}}{=} 0$, $|K_0\rangle \stackrel{\text{def}}{=} |\psi(0)\rangle$, $|K_{-1}\rangle \stackrel{\text{def}}{=} 0$, and $a_n \stackrel{\text{def}}{=} \langle K_n | H | K_n \rangle$. The quantities a_n and b_n in Eq. (12) are known as Lanczos coefficients. Manipulation of the two relations in Eq. (12) yields

$$H |K_n\rangle = b_{n+1} |K_{n+1}\rangle + a_n |K_n\rangle + b_n |K_{n-1}\rangle. \quad (13)$$

Therefore, given Eq. (13), the Hamiltonian H is tridiagonal with respect to the Krylov basis. In particular, the tridiagonal elements are given by the Lanczos coefficients. For completeness, we remark that the Gram-Schmidt and Lanczos algorithms are not the same. However, the Lanczos algorithm can be viewed as an efficient version of the Gram-Schmidt algorithm tailored to Krylov spaces and Hermitian operators. It is noteworthy that the conventional Krylov construction utilizing the Lanczos algorithm is applicable solely to autonomous Hamiltonian systems, which possess a constant Hamiltonian. For an extension of the Krylov construction to periodically driven systems, also known as Floquet systems [42, 43], where the Lanczos algorithm is substituted with the Arnoldi iteration [44], we direct the reader to Refs. [45, 46]. In this periodic setting, we wish to highlight that the (Hermitian) Hamiltonian operator H is substituted with the (unitary) Floquet operator U_F of the system during the formation of Krylov's basis, with $\{H^n |\psi(0)\rangle\} \rightarrow \{U_F^n |\psi(0)\rangle\}$ [45].

The fundamental concept behind Krylov's state complexity is the expectation that a more intricate time evolution will distribute $|\psi(t)\rangle$ more extensively across the Hilbert space in comparison to the initial state $|\psi(0)\rangle$. The degree of this distribution is influenced by the selected basis. Nevertheless, one can assess the complexity of the evolution by minimizing the wavefunction's spread across all bases. To measure this spread, one should consider a cost function $C_B(t)$ in relation to a complete, orthonormal, ordered basis, $\mathcal{B} = \{B_n\}$ for the Hilbert space provided by

$$C_B(t) = \sum_n c_n |\langle \psi(t) | B_n \rangle|^2 = \sum_n c_n p_B(n, t), \quad (14)$$

with $\sum_n p_B(n, t) = 1$. The quantity c_n is a positive, increasing sequence of real-valued numbers, and $p_B(n, t)$ are the probabilities of being in each basis vector. In general, one takes $c_n = n$ so that $C_B(t)$ in Eq. (14) measures the

average spread of $|\psi(0)\rangle$ in the basis \mathcal{B} . Finally, Krylov's state complexity is defined as [11, 17, 18, 47]

$$\mathcal{K}(t) \stackrel{\text{def}}{=} \min_{\mathcal{B}} \text{C}_{\mathcal{B}}(t), \quad (15)$$

that is,

$$\begin{aligned} \mathcal{K}(t) &= \sum_n c_n |\langle \psi(t) | K_n \rangle|^2 \\ &= \langle \psi(t) | \hat{K} | \psi(t) \rangle \\ &= \sum_n n p_{\mathcal{K}}(n, t), \end{aligned} \quad (16)$$

where \hat{K} is the K -complexity operator. From Eq. (16), we note that $\mathcal{K}(t)$ can be viewed as the expectation value of the K -complexity operator with respect to the state $|\psi(t)\rangle$ or, alternatively, as the average of n in the probability distribution $p_{\mathcal{K}}(n, t) = |\langle \psi(t) | K_n \rangle|^2$. For simplicity of notation, we use $p_n(t)$ instead of $p_{\mathcal{K}}(n, t)$ in the remaining of the paper. By construction, $\mathcal{K}(0) = 0$ and $\mathcal{K}(t) \geq 0$ for $t > 0$. Krylov's state complexity $\mathcal{K}(t)$ measures how far the state $|\psi(0)\rangle$ has evolved under H away from the initial site with $n = 0$ ($\leftrightarrow |K_0\rangle$) along the $1D$ chain/lattice whose sites $n > 0$ label increasingly complex Krylov states $|K_n\rangle$. The selection of the Krylov basis for measuring the spread is determined by its ability to establish a direction in which complexity is reduced, particularly near $t = 0$. In Fig. 3, we show a visual representation that aids in understanding the concept of Krylov's state complexity in both lower and higher complexity level scenarios.

We emphasize that Krylov's state complexity is constructed from the basis that produces the least spread, as this is the only scenario in which complexity accurately represents the inevitable growth dictated by the Hamiltonian, rather than being a by-product of the chosen basis. While it is possible to utilize a maximally spreading basis, the outcome is not a significant interpretation of complexity; instead, it becomes a coordinate-dependent distortion. Complexity ought to be an attribute of the dynamics, independent of the observer's coordinate framework. The Krylov basis is determined canonically by the dynamics through the Lanczos algorithm, eliminating arbitrary basis freedom. It assesses the intrinsic spread of states related to the Hamiltonian, rather than the artificial delocalization resulting from an inadequate basis selection. Furthermore, it establishes a lower bound on the complexity that the dynamics must exhibit. For further details on the Krylov state complexity, we suggest Ref. [11].

In the following subsection, we introduce our quantum information geometry measure of complexity.

B. Quantum information geometry complexity

In furtherance of the research detailed in Refs. [19, 20], we evaluate the single-qubit quantum dynamics influenced by both stationary and nonstationary Hamiltonian evolutions across a specified time interval $[t_A, t_B]$, by establishing the complexity $\text{C}(t_A, t_B)$ as

$$\text{C}(t_A, t_B) \stackrel{\text{def}}{=} \frac{\text{V}_{\max}(t_A, t_B) - \bar{\text{V}}(t_A, t_B)}{\text{V}_{\max}(t_A, t_B)}. \quad (17)$$

The reasoning for suggesting this expression for the complexity $\text{C}(t_A, t_B)$ will be clarified in the following paragraphs.

We begin by defining $\bar{\text{V}}(t_A, t_B)$ and $\text{V}_{\max}(t_A, t_B)$ as outlined in Eq. (17). To clarify the definition of the so-called *accessed volume* $\bar{\text{V}}(t_A, t_B)$, we will utilize a schematic approach as follows. If possible, analytically integrate the time-dependent Schrödinger evolution equation $i\hbar\partial_t |\psi(t)\rangle = H(t) |\psi(t)\rangle$ and express the (normalized) single-qubit state vector $|\psi(t)\rangle$ at any arbitrary time t in terms of the computational basis state vectors $\{|0\rangle, |1\rangle\}$. If this is not achievable, proceed with a numerical analysis. We derive $|\psi(t)\rangle = c_0(t)|0\rangle + c_1(t)|1\rangle$, where $c_0(t)$ and $c_1(t)$ are reformulated as

$$c_0(t) \stackrel{\text{def}}{=} \langle 0 | \psi(t) \rangle = |c_0(t)| e^{i\phi_0(t)}, \text{ and } c_1(t) \stackrel{\text{def}}{=} \langle 1 | \psi(t) \rangle = |c_1(t)| e^{i\phi_1(t)}, \quad (18)$$

respectively. Moreover, it is crucial to recognize that $\phi_0(t)$ and $\phi_1(t)$ represent the real-valued phases of $c_0(t)$ and $c_1(t)$, respectively. Following this, by employing the complex quantum amplitudes $c_0(t)$ and $c_1(t)$ as outlined in Eq. (18), reformulate the state $|\psi(t)\rangle$ into a physically equivalent state articulated in its standard Bloch sphere representation, which is characterized by the polar angle $\theta(t) \in [0, \pi]$ and the azimuthal angle $\varphi(t) \in [0, 2\pi]$. With the temporal

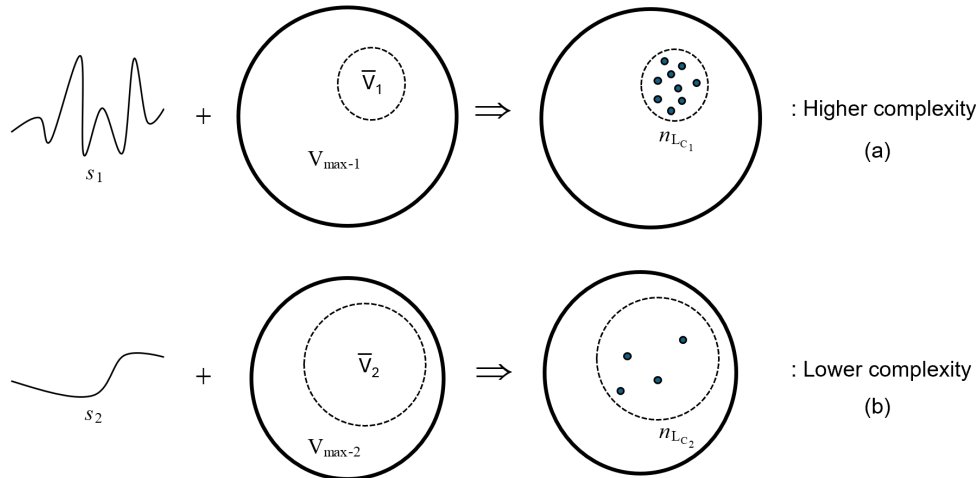


FIG. 4: A visual representation that aids in understanding the concept of complexity $C(t_A, t_B)$ with $t_A \leq t \leq t_B$. In (a), we illustrate a complex situation where the accessed volume \bar{V}_1 (the area enclosed by the dashed circular line) constitutes a minor portion of the total accessible volume $V_{\max-1}$ (the area enclosed by the thick solid circular line). Conversely, in (b), we depict a scenario with a reduced level of complexity, as \bar{V}_2 (the area enclosed by the dashed circular line) represents a larger portion of $V_{\max-2}$ (the area enclosed by the thick solid circular line). The length s of a path serves as an estimate for the maximum number n_s of statistically distinguishable states along that path. Generally, the higher complexity scenario in (a) corresponds to a longer quantum path of length s_1 , characterized by a small fraction $(\bar{V}_1/V_{\max-1})$ of the total accessible volume $V_{\max-1}$. In contrast, the lower complexity scenario in (b) typically corresponds to a shorter quantum path of length $s_2 < s_1$, described by a larger fraction $(\bar{V}_2/V_{\max-2})$, with $\bar{V}_2/V_{\max-2} > \bar{V}_1/V_{\max-1}$ of the total accessible volume $V_{\max-2}$. The number n_{LC} of points represented in an accessed volume \bar{V} is proportional to the square of the length s^2 of the path, enhanced by a factor that is the reciprocal of \bar{V}/V_{\max} , where $0 \leq \bar{V}/V_{\max} \leq 1$. These two scenarios in (a) and (b) are accurately characterized by the concept of complexity length scale L_C , with $n_{LC} \stackrel{\text{def}}{=} L_C^2 = s^2 \cdot (\bar{V}/V_{\max})^{-1}$ [19, 20].

variations of the two spherical angles $\theta(t)$ and $\varphi(t)$ at hand, ascertain the volume of the parametric region that the quantum-mechanical system navigates during its evolution from $|\psi(t_A)\rangle = |A\rangle$ to $|\psi(t)\rangle$. Lastly, calculate the temporal-average volume of the parametric region traversed by the quantum-mechanical system as it transitions from $|\psi(t_A)\rangle = |A\rangle$ to $|\psi(t_B)\rangle = |B\rangle$ with $t \in [t_A, t_B]$.

In alignment with this initial framework, we will now delve into the specifics of the calculation process for $\bar{V}(t_A, t_B)$. By employing Eq. (18), we note that $|\psi(t)\rangle = c_0(t)|0\rangle + c_1(t)|1\rangle$ is physically analogous to the state $|c_0(t)|0\rangle + |c_1(t)|e^{i[\phi_1(t) - \phi_0(t)]}|1\rangle$. As a result, $|\psi(t)\rangle$ can be redefined as

$$|\psi(t)\rangle = \cos\left[\frac{\theta(t)}{2}\right]|0\rangle + e^{i\varphi(t)}\sin\left[\frac{\theta(t)}{2}\right]|1\rangle. \quad (19)$$

From a formal standpoint, the polar angle $\theta(t)$ and the azimuthal angle $\varphi(t) \stackrel{\text{def}}{=} \phi_1(t) - \phi_0(t) = \arg[c_1(t)] - \arg[c_0(t)]$ as stated in Eq. (19) can be articulated as

$$\theta(t) \stackrel{\text{def}}{=} 2 \arctan\left(\frac{|c_1(t)|}{|c_0(t)|}\right), \quad (20)$$

and, assuming that $\text{Re}[c_1(t)] > 0$ and $\text{Re}[c_0(t)] > 0$,

$$\varphi(t) \stackrel{\text{def}}{=} \arctan\left\{\frac{\text{Im}[c_1(t)]}{\text{Re}[c_1(t)]}\right\} - \arctan\left\{\frac{\text{Im}[c_0(t)]}{\text{Re}[c_0(t)]}\right\}, \quad (21)$$

respectively.

In general, the functional representation of $\varphi(t)$ as outlined in Eq. (21) can take on a more intricate expression. This complexity stems from the need to articulate the phase $\arg(z)$ of a complex number $\mathbb{C} \ni z \stackrel{\text{def}}{=} x + iy = |z|e^{i\arg(z)}$ using the 2-argument arctangent function atan2 as $\arg(z) = \text{atan2}(y, x)$. When $x > 0$, the function $\text{atan2}(y, x)$ reduces to $\arctan(y/x)$. For additional mathematical perspectives on atan2 , we suggest referring to Ref. [48]. Consequently, with $\theta(t)$ and $\varphi(t)$ established, it can be noted that the unit three-dimensional Bloch vector $\mathbf{a}(t)$, which corresponds

to the state vector $|\psi(t)\rangle$ as specified in Eq. (19), is represented as $\mathbf{a}(t) = (\sin[\theta(t)]\cos[\varphi(t)], \sin[\theta(t)]\sin[\varphi(t)], \cos[\theta(t)])$. Currently, we can define $\bar{V}(t_A, t_B)$. Specifically, the accessed volume $\bar{V}(t_A, t_B)$, which pertains to the quantum evolution governed by the Hamiltonian $H(t)$ from $|\psi(t_A)\rangle = |A\rangle$ to $|\psi(t_B)\rangle = |B\rangle$, where t lies within the interval $[t_A, t_B]$, is expressed as

$$\bar{V}(t_A, t_B) \stackrel{\text{def}}{=} \frac{1}{t_B - t_A} \int_{t_A}^{t_B} V(t) dt. \quad (22)$$

Eq. (22) implies that $\bar{V}(t_A, t_B)$ can be viewed as a mean value of $V(t)$ calculated over the time interval $[t_A, t_B]$. The quantity $V(t)$ in Eq. (22) is the instantaneous volume, which is given by

$$V(t) = V(\theta(t), \varphi(t)) \stackrel{\text{def}}{=} \text{vol}[\mathcal{D}_{\text{accessed}}[\theta(t), \varphi(t)]], \quad (23)$$

where $\text{vol}[\mathcal{D}_{\text{accessed}}[\theta(t), \varphi(t)]]$ is defined as

$$\text{vol}[\mathcal{D}_{\text{accessed}}[\theta(t), \varphi(t)]] \stackrel{\text{def}}{=} \int \int_{\mathcal{D}_{\text{accessed}}[\theta(t), \varphi(t)]} \sqrt{g_{\text{FS}}(\theta, \varphi)} d\theta d\varphi. \quad (24)$$

We stress that $\text{vol}[\cdot]$ signifies $|\text{vol}[\cdot]| \geq 0$, given that volumes as defined by positive real-valued numerical values. In Eq. (24), $g_{\text{FS}}(\theta, \varphi) \stackrel{\text{def}}{=} \sqrt{\sin^2(\theta)/16}$ denotes the determinant of the matrix connected to the Fubini-Study infinitesimal line element $ds_{\text{FS}}^2 \stackrel{\text{def}}{=} (1/4)[d\theta^2 + \sin^2(\theta)d\varphi^2]$. Lastly, $\mathcal{D}_{\text{accessed}}[\theta(t), \varphi(t)]$ in Eq. (24) represents the parametric region that the quantum system explores as it transitions from the initial state $|\psi(t_A)\rangle = |A\rangle$ to an intermediate state $|\psi(t)\rangle$, where $t_A \leq t \leq t_B$. It is given by

$$\mathcal{D}_{\text{accessed}}[\theta(t), \varphi(t)] \stackrel{\text{def}}{=} [\theta(t_A), \theta(t)] \times [\varphi(t_A), \varphi(t)] \subset [0, \pi]_\theta \times [0, 2\pi]_\varphi. \quad (25)$$

To improve computational efficiency, we note that the instantaneous volume $V(t)$ in Eq. (23) can be conveniently reformulated as $V(t) = |(\cos[\theta(t_A)] - \cos[\theta(t)]) (\varphi(t) - \varphi(t_A))|/4$, where $\theta(t)$ and $\varphi(t)$ are defined Eqs. (20) and (21), respectively. In summary, assuming that the tilde symbol represents the time-average process, the accessed volume $\bar{V}(t_A, t_B)$ in Eq. (22) can be recast as

$$\bar{V}(t_A, t_B) \stackrel{\text{def}}{=} \tilde{\text{vol}}[\mathcal{D}_{\text{accessed}}[\theta(t), \varphi(t)]], \quad (26)$$

where $t_A \leq t \leq t_B$ in Eq. (26). Ultimately, in alignment with the physical justifications outlined in Refs. [19, 20], the accessible volume $V_{\text{max}}(t_A, t_B)$ in Eq. (17) is given by

$$V_{\text{max}}(t_A, t_B) \stackrel{\text{def}}{=} \text{vol}[\mathcal{D}_{\text{accessible}}(\theta, \varphi)] = \int \int_{\mathcal{D}_{\text{accessible}}(\theta, \varphi)} \sqrt{g_{\text{FS}}(\theta, \varphi)} d\theta d\varphi. \quad (27)$$

The quantity $\mathcal{D}_{\text{accessible}}(\theta, \varphi)$ in Eq. (27) is the (local) maximally accessible two-dimensional parametric region that characterizes the quantum-mechanical transition from $|\psi_A(\theta_A, \varphi_A)\rangle$ to $|\psi(\theta_B, \varphi_B)\rangle$ and is expressed by

$$\mathcal{D}_{\text{accessible}}(\theta, \varphi) \stackrel{\text{def}}{=} \{(\theta, \varphi) : \theta_{\text{min}} \leq \theta \leq \theta_{\text{max}}, \text{ and } \varphi_{\text{min}} \leq \varphi \leq \varphi_{\text{max}}\}. \quad (28)$$

It is relevant to notice that θ_{min} , θ_{max} , φ_{min} , and φ_{max} in Eq. (28) are defined as

$$\theta_{\text{min}} \stackrel{\text{def}}{=} \min_{t_A \leq t \leq t_B} \theta(t), \theta_{\text{max}} \stackrel{\text{def}}{=} \max_{t_A \leq t \leq t_B} \theta(t), \varphi_{\text{min}} \stackrel{\text{def}}{=} \min_{t_A \leq t \leq t_B} \varphi(t), \text{ and } \varphi_{\text{max}} \stackrel{\text{def}}{=} \max_{t_A \leq t \leq t_B} \varphi(t), \quad (29)$$

respectively. Furthermore, it is important to note that $\mathcal{D}_{\text{accessed}}(\theta, \varphi) \subset \mathcal{D}_{\text{accessible}}(\theta, \varphi) \subset [0, \pi]_\theta \times [0, 2\pi]_\varphi$. Finally, given $\bar{V}(t_A, t_B)$ and $V_{\text{max}}(t_A, t_B)$ as defined in Eqs. (22) and (27), respectively, we can establish our proposed complexity concept $C(t_A, t_B)$ as outlined in Eq. (17).

In broad terms, we evaluate the complexity of a quantum evolution transitioning from an initial state to a final state on the Bloch sphere by examining the ratio of the unaccessed volume of the sphere that is contained within the accessible volume of the sphere itself. In particular, when the accessible volume is largely (minimally) explored, the complexity is considered low (high). In Fig. 4, we present a visual depiction that facilitates comprehension of our quantum IG measure of complexity across both lower and higher complexity level scenarios. For further information, we direct you to Refs. [19, 20].

To enhance the efficacy of our comparative analysis, we will reframe Krylov's state complexity in relation to the overlaps of simple three-dimensional real-valued vectors that define the characteristics of the qubit dynamics under examination.

IV. GEOMETRY OF KRYLOV'S STATE COMPLEXITY

In this section, we rephrase both the instantaneous and time-averaged Krylov state complexity for stationary and nonstationary Hamiltonian evolutions, depicting them using two real-valued vectors that have distinct geometric importance.

A. Stationary qubit dynamics

Here, we calculate the general expression of Krylov's state complexity $\mathcal{K}(t)$ in the case in which the qubit dynamics are governed by a stationary Hamiltonian. In particular, the expression is geometric since it can be fully expressed in terms of the relative geometry of just two real vectors, the initial Bloch vector of the system $\mathbf{a}(t_i)$ and the time independent magnetic field vector \mathbf{h} that specifies the (generally non traceless) Hamiltonian $H \stackrel{\text{def}}{=} h_0 \mathbf{1} + \mathbf{h} \cdot \boldsymbol{\sigma}$.

We begin by assuming a Hamiltonian given by $H \stackrel{\text{def}}{=} h_0 \mathbf{1} + \mathbf{h} \cdot \boldsymbol{\sigma}$ and, moreover, we take the initial state $|\psi(t_i)\rangle = |\psi(0)\rangle$ of the quantum system to be arbitrarily given by $|\psi(0)\rangle \stackrel{\text{def}}{=} \cos(\theta_0/2)|0\rangle + e^{i\varphi_0}\sin(\theta_0/2)|1\rangle$. Therefore, after some algebra, we find that the expression of the unitarily time-evolved unit state vector $|\psi(t)\rangle = U(t)|\psi(0)\rangle = e^{-\frac{i}{\hbar}[h_0\mathbf{1}+\mathbf{h}\cdot\boldsymbol{\sigma}]}|\psi(0)\rangle$ with $U(t) \stackrel{\text{def}}{=} e^{-\frac{i}{\hbar}h_0t}[\cos(\frac{ht}{\hbar})\mathbf{1} - i\sin(\frac{ht}{\hbar})\mathbf{n}\cdot\boldsymbol{\sigma}]$, $\mathbf{h} \stackrel{\text{def}}{=} h\mathbf{n}$, and $h \stackrel{\text{def}}{=} \|\mathbf{h}\|$ is given by

$$|\psi(t)\rangle = e^{-\frac{i}{\hbar}h_0t} \left[\cos\left(\frac{ht}{\hbar}\right)\mathbf{1} - i\sin\left(\frac{ht}{\hbar}\right)\mathbf{n}\cdot\boldsymbol{\sigma} \right] |\psi(0)\rangle. \quad (30)$$

In the orthonormal Krylov basis $\{|\phi_0\rangle = |\psi(0)\rangle, |\phi_1\rangle = |\psi_{\perp}(0)\rangle\}$, we have

$$|\psi(t)\rangle = \langle\psi(0)|\psi(t)\rangle|\psi(0)\rangle + \langle\psi_{\perp}(0)|\psi(t)\rangle|\psi_{\perp}(0)\rangle, \quad (31)$$

where $|\langle\psi(0)|\psi(t)\rangle|^2 + |\langle\psi_{\perp}(0)|\psi(t)\rangle|^2 = 1$. Therefore, the expression of Krylov's state complexity becomes

$$\begin{aligned} \mathcal{K}(t) &= \sum_{n=0}^1 np_n(t) = \sum_{n=0}^1 n |\langle\phi_n|\psi(t)\rangle|^2 = |\langle\phi_1|\psi(t)\rangle|^2 = 1 - |\langle\phi_0|\psi(t)\rangle|^2 \\ &= 1 - |\langle\psi(0)|\psi(t)\rangle|^2 = 1 - |\langle\psi(0)|U(t)|\psi(0)\rangle|^2, \end{aligned} \quad (32)$$

that is,

$$\mathcal{K}(t) = 1 - |\langle\psi(0)|U(t)|\psi(0)\rangle|^2. \quad (33)$$

Let us then find a convenient form for the quantum overlap $\langle\psi(0)|U(t)|\psi(0)\rangle$ and, consequently, a geometrically relevant expression for the probability $|\langle\psi(0)|U(t)|\psi(0)\rangle|^2$. Given that,

$$\langle\psi(0)|U(t)|\psi(0)\rangle = e^{-\frac{i}{\hbar}h_0t} \left[\cos\left(\frac{ht}{\hbar}\right) - i\sin\left(\frac{ht}{\hbar}\right) \langle\psi(0)|\mathbf{n}\cdot\boldsymbol{\sigma}|\psi(0)\rangle \right], \quad (34)$$

noting that $\langle\psi(0)|\boldsymbol{\sigma}|\psi(0)\rangle = \mathbf{a}(t_i)$ (i.e., it is the Bloch vector of the initial state $|\psi(0)\rangle$ with $t_i = 0$), we finally arrive at

$$\mathcal{K}(t) = \sin^2\left(\frac{ht}{\hbar}\right) \left\{ 1 - [\mathbf{n}\cdot\mathbf{a}(t_i)]^2 \right\}, \quad (35)$$

with $\mathbf{a}(t_i) = (\sin(\theta_{t_i})\cos(\varphi_{t_i}), \sin(\theta_{t_i})\sin(\varphi_{t_i}), \cos(\theta_{t_i}))$. Eq. (35) represents the geometric expression for $\mathcal{K}(t)$ we were looking for. Observe that, as expected on physics grounds, $\mathcal{K}(t)$ in Eq. (35) does not depend on h_0 . Interestingly, observe that when \mathbf{n} and $\mathbf{a}(t_i)$ are collinear, the initial state of the system is an eigenstate of the Hamiltonian H . Therefore, there is no evolution and $\mathcal{K}(t)$ vanishes. Moreover, when \mathbf{n} is orthogonal to $\mathbf{a}(t_i)$, one achieves the maximal “instantaneous” Krylov state complexity with $\mathcal{K}(t) = \sin^2(ht/\hbar)$. Finally, when \mathbf{n} is not orthogonal to $\mathbf{a}(t_i)$, one achieves a sub-maximal “instantaneous” Krylov state complexity with $\mathcal{K}(t) \leq \sin^2(ht/\hbar)$. It is important to stress that Eq. (35) is valid only in the stationary case in which H does not depend on time. It is worth pointing out that using Eq. (35) along with the mathematical identity

$$\frac{1}{T} \int_0^T \sin^2\left(\frac{ht}{\hbar}\right) dt = \frac{1}{2} - \frac{\sin\left(\frac{2hT}{\hbar}\right)}{\frac{4hT}{\hbar}}, \quad (36)$$

we have that in the case of geodesic motion $\mathbf{n} \cdot \mathbf{a}(t_i) = 0$ and $\langle \mathcal{K} \rangle_{\text{geo}}$ becomes

$$\langle \mathcal{K} \rangle_{\text{geo}} = \frac{1}{2} - \frac{\sin\left(\frac{2ht_f^{\text{geo}}}{\hbar}\right)}{\frac{4ht_f^{\text{geo}}}{\hbar}}. \quad (37)$$

Furthermore, in the case of nongeodesic motion, $\mathbf{n} \cdot \mathbf{a}(t_i) \neq 0$ and $\langle \mathcal{K} \rangle_{\text{nongeo}}$ reduces to

$$\langle \mathcal{K} \rangle_{\text{nongeo}} = \left\{ 1 - [\mathbf{n} \cdot \mathbf{a}(t_i)]^2 \right\} \left[\frac{1}{2} - \frac{\sin\left(\frac{2ht_f^{\text{nongeo}}}{\hbar}\right)}{\frac{4ht_f^{\text{nongeo}}}{\hbar}} \right]. \quad (38)$$

The interested reader can verify that considering the specific proper expressions for \mathbf{n} , $\mathbf{a}(t_i)$, h , t_f^{geo} , and t_f^{nongeo} , $\langle \mathcal{K} \rangle_{\text{geo}}$ in Eq. (37) yields Eq. (59), while $\langle \mathcal{K} \rangle_{\text{nongeo}}$ in Eq. (38) leads to Eq. (65). With these final remarks, we end our discussion here.

B. Nonstationary qubit dynamics

Here, we find the general expression of Krylov's state complexity $\mathcal{K}(t)$ when the qubit dynamics are specified by a nonstationary Hamiltonian. Specifically, the expression is geometric in nature because it can be fully characterized by means of the relative geometry of just two real-valued vectors, the initial and the time-evolved Bloch vectors of the system $\mathbf{a}(t_i)$ and $\mathbf{a}(t)$, respectively. Without loss of generality, we assume $\mathbf{H}(t) \stackrel{\text{def}}{=} \mathbf{h}(t) \cdot \boldsymbol{\sigma}$ with $\mathbf{h}(t) \stackrel{\text{def}}{=} h(t) \mathbf{n}(t)$ and $h(t) \stackrel{\text{def}}{=} \|\mathbf{h}(t)\|$ as mentioned in the previous subsection.

The main objective is to derive the analog of $\mathcal{K}(t)$ in Eq. (35) when $\mathbf{H} = \mathbf{H}(t)$. From Eq. (33), setting $\rho(0) \stackrel{\text{def}}{=} |\psi(0)\rangle\langle\psi(0)| = [\mathbf{1} + \mathbf{a}(0) \cdot \boldsymbol{\sigma}] / 2$ and $\rho(t) \stackrel{\text{def}}{=} |\psi(t)\rangle\langle\psi(t)| = [\mathbf{1} + \mathbf{a}(t) \cdot \boldsymbol{\sigma}] / 2$ and after some standard algebra of Pauli matrices, we get

$$\begin{aligned} \mathcal{K}(t) &= 1 - |\langle\psi(0)|U(t)|\psi(0)\rangle|^2 \\ &= 1 - |\langle\psi(0)|\psi(t)\rangle|^2 \\ &= 1 - \text{tr}[\rho(0)\rho(t)] \\ &= 1 - \text{tr}\left[\left(\frac{\mathbf{1} + \mathbf{a}(0) \cdot \boldsymbol{\sigma}}{2}\right)\left(\frac{\mathbf{1} + \mathbf{a}(t) \cdot \boldsymbol{\sigma}}{2}\right)\right] \\ &= 1 - \frac{1}{2}[1 + \mathbf{a}(0) \cdot \mathbf{a}(t)] \\ &= \frac{1}{2}[1 - \mathbf{a}(0) \cdot \mathbf{a}(t)] \\ &= \frac{1}{2}[1 - \mathbf{a}(0) \cdot \mathcal{R}(t)\mathbf{a}(0)], \end{aligned} \quad (39)$$

that is,

$$\mathcal{K}(t) = \frac{1}{2}[1 - \mathbf{a}(0) \cdot \mathcal{R}(t)\mathbf{a}(0)]. \quad (40)$$

For completeness, we note that $|\langle\psi(0)|U(t)|\psi(0)\rangle|^2$ is known as the survival probability (i.e., the probability that the system is still in the initial state at time t), while $1 - |\langle\psi(0)|U(t)|\psi(0)\rangle|^2$ is the complement of the survival probability known as decay probability (or, alternatively, fidelity loss or escape probability). The emergence of the rotation matrix $\mathcal{R}(t)$ in Eq. (40) is due to the fact that every unitary time propagator $U(t) \in \text{SU}(2; \mathbb{C})$ induces a unique rotation matrix $\mathcal{R}(t) \in \text{SO}(3; \mathbb{R})$ acting on Bloch vectors [49–51], such that $\rho(t) = U(t)\rho(0)U^\dagger(t) \leftrightarrow \mathbf{a}(t) = \mathcal{R}(t)\mathbf{a}(0)$. From Eq. (40), the time averaged Krylov state complexity is formally given by

$$\langle \mathcal{K}(t) \rangle = \frac{1}{2}[1 - \langle \mathbf{a}(0) \cdot \mathcal{R}(t)\mathbf{a}(0) \rangle], \quad (41)$$

therefore, $\langle \mathcal{K}(t) \rangle$ depends on $\langle \mathbf{a}(0) \cdot \mathbf{a}(t) \rangle$. Eqs. (40) and (41) are valid for both stationary and nonstationary quantum mechanical Hamiltonian evolutions.

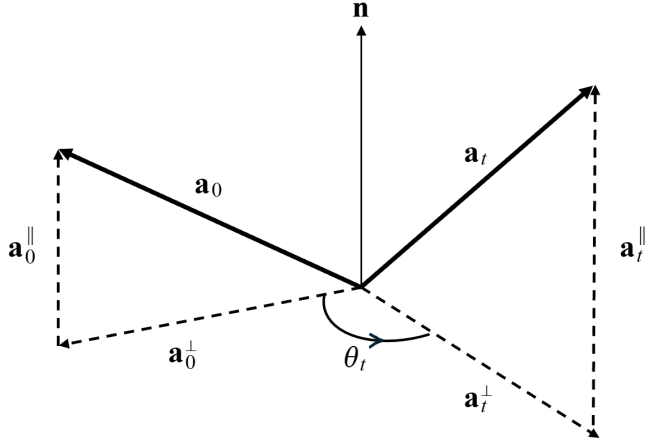


FIG. 5: Geometric sketch for Rodrigues' rotation formula, $\mathbf{a}_t = \mathcal{R}_n(\theta_t) \mathbf{a}_0$ with $\mathbf{a}_0 \stackrel{\text{def}}{=} \mathbf{a}_0^{\parallel} + \mathbf{a}_0^{\perp}$ and $\mathbf{a}_t \stackrel{\text{def}}{=} \mathbf{a}_t^{\parallel} + \mathbf{a}_t^{\perp}$. We stress that $\mathcal{R}_n(\theta_t)$ denotes a rotation about the axis specified by means of the unit vector \mathbf{n} by an angle θ_t .

Interestingly, one can recover Eq. (35) from Eq. (40) when H is stationary. Before examining this, let us set $\mathbf{a}(0) = \mathbf{a}_0$ and $\mathbf{a}(t) = \mathbf{a}_t$ for simplicity of notation. Then, start considering the decomposition of \mathbf{a}_0 as

$$\mathbf{a}_0 = \mathbf{a}_0^{\parallel} + \mathbf{a}_0^{\perp}, \quad (42)$$

where $\mathbf{a}_0^{\parallel} = (\mathbf{a}_0 \cdot \mathbf{n}) \mathbf{n}$ is the vectorial part of \mathbf{a}_0 that is parallel to \mathbf{n} and, in addition, $\mathbf{a}_0^{\perp} = \mathbf{a}_0 - (\mathbf{a}_0 \cdot \mathbf{n}) \mathbf{n}$ is the vectorial part of \mathbf{a}_0 that is orthogonal to \mathbf{n} . We stress that $\mathbf{a}_0^{\parallel} \cdot \mathbf{a}_0^{\perp} = 0$ and $\|\mathbf{a}_0\|^2 = \|\mathbf{a}_0^{\parallel}\|^2 + \|\mathbf{a}_0^{\perp}\|^2 = 1$. We also remark that $\mathcal{R}(t)$ leaves the parallel component invariant since $\mathcal{R}(t) \mathbf{a}_0^{\parallel} = \mathbf{a}_0^{\parallel}$ and, in addition,

$$\mathcal{R}(t) \mathbf{a}_0^{\perp} = \mathbf{a}_0^{\perp} \cos\left(\frac{2h}{\hbar}t\right) + (\mathbf{n} \times \mathbf{a}_0^{\perp}) \sin\left(\frac{2h}{\hbar}t\right). \quad (43)$$

Eq. (43) implies that the perpendicular component \mathbf{a}_0^{\perp} rotates in the plane orthogonal to \mathbf{n} by an angle $(2h/\hbar)t$. This is an ordinary result of rigid rotations in \mathbb{R}^3 . For later convenience, we also remark that $\mathbf{a}_0 \in \text{Span}\{\mathbf{n}, \mathbf{a}_0^{\perp}\}$ and, consequently, $\mathbf{a}_0 \cdot (\mathbf{n} \times \mathbf{a}_0^{\perp}) = 0$. Having presented these properties, we proceed with the manipulation of $\mathcal{K}(t)$ in Eq. (40). We have,

$$\begin{aligned} \mathbf{a}_0 \cdot \mathcal{R}(t) \mathbf{a}_0 &= (\mathbf{a}_0^{\parallel} + \mathbf{a}_0^{\perp}) \cdot [\mathcal{R}(t) (\mathbf{a}_0^{\parallel} + \mathbf{a}_0^{\perp})] \\ &= (\mathbf{a}_0^{\parallel} + \mathbf{a}_0^{\perp}) \cdot \left[\mathbf{a}_0^{\parallel} + \mathbf{a}_0^{\perp} \cos\left(\frac{2h}{\hbar}t\right) + (\mathbf{n} \times \mathbf{a}_0^{\perp}) \sin\left(\frac{2h}{\hbar}t\right) \right] \\ &= \|\mathbf{a}_0^{\parallel}\|^2 + \|\mathbf{a}_0^{\perp}\|^2 \cos\left(\frac{2h}{\hbar}t\right) \\ &= (\mathbf{a}_0 \cdot \mathbf{n})^2 + \left[1 - (\mathbf{a}_0 \cdot \mathbf{n})^2 \right] \cos\left(\frac{2h}{\hbar}t\right) \end{aligned} \quad (44)$$

and, therefore

$$\begin{aligned} \mathcal{K}(t) &= \frac{1}{2} [1 - \mathbf{a}_0 \cdot \mathcal{R}(t) \mathbf{a}_0] \\ &= \frac{1}{2} \left\{ 1 - (\mathbf{a}_0 \cdot \mathbf{n})^2 - \left[1 - (\mathbf{a}_0 \cdot \mathbf{n})^2 \right] \cos\left(\frac{2h}{\hbar}t\right) \right\} \\ &= \frac{1 - \cos\left(\frac{2h}{\hbar}t\right)}{2} \left[1 - (\mathbf{a}_0 \cdot \mathbf{n})^2 \right] \\ &= \sin^2\left(\frac{h}{\hbar}t\right) \left[1 - (\mathbf{a}_0 \cdot \mathbf{n})^2 \right]. \end{aligned} \quad (45)$$

We finally conclude that $\mathcal{K}(t)$ in Eq. (45) coincides with $\mathcal{K}(t)$ in Eq. (35) and, as a consequence, Eq. (35) is a special case of Eq. (40). In Fig. 5, we provide a visual representation that aids in understanding the Rodrigues rotation formula. For a step-by-step derivation of the explicit expression of the rotation matrix $\mathcal{R}(t)$ in Eq. (45), we refer to Appendix B. With this final comment, we conclude this technical subsection here.

C. Difference between stationary and nonstationary qubit dynamics

Here, we discuss an essential difference in the behavior of Krylov's state complexity when one transitions from stationary to nonstationary Hamiltonian evolutions. Specifically, unlike what happens in a time independent setting, we show that the orthogonality between the unit vectors \mathbf{n} and \mathbf{a}_0 (with $H(t) \stackrel{\text{def}}{=} \mathbf{h}(t) \cdot \boldsymbol{\sigma}$, $\mathbf{h}(t) \stackrel{\text{def}}{=} h(t) \mathbf{n}(t)$, and $\rho(0) \stackrel{\text{def}}{=} |\psi(0)\rangle \langle \psi(0)| = [\mathbf{1} + \mathbf{a}_0 \cdot \boldsymbol{\sigma}] / 2$) does not generally imply that $\mathcal{K}(t)$ achieves its maximal instantaneous value. In other words, it can happen that there is no time instance in which $\mathcal{K}(t)$ equals one or, put differently, the evolving state vector $|\psi(t)\rangle$ never gets fully orthogonal to the initial state $|\psi(0)\rangle$.

1. Preliminaries

Before presenting our physical example where the above mentioned difference becomes evident, we illustrate some preliminary remarks.

From an historical standpoint, we remark that Rabi [52, 53] was a pioneer in applying the rotating frame concept within quantum mechanics, specifically for magnetic resonance, during his molecular beam experiments in the 1930s, which focused on measuring nuclear magnetic moments. His research demonstrated how a rotating magnetic field can facilitate the comprehension of transitions in a static field, laying the groundwork for the rotating wave approximation and proving essential for NMR (nuclear magnetic resonance) and quantum control. Notably, he proposed the concept of a rotating coordinate system that aligns with the oscillating magnetic field, thereby significantly simplifying the visualization and resolution of the time-dependent problem of spin transitions, particularly in proximity to resonance.

From a practical standpoint, assume that the unitary time propagator $U(t)$ describes the evolution in the laboratory frame of reference and is associated with the Hamiltonian $H(t)$. In the laboratory, Schrödinger's evolution equation is $i\hbar\partial_t |\psi(t)\rangle = H(t) |\psi(t)\rangle$. In the rotating reference frame, instead, suppose that the unitary time evolution is characterized by the operator $U_{\text{RF}}(t)$ that corresponds to the Hamiltonian $H_{\text{RF}}(t)$. In the rotating frame of reference, Schrödinger's evolution equation is $i\hbar\partial_t |\psi_{\text{RF}}(t)\rangle = H_{\text{RF}}(t) |\psi_{\text{RF}}(t)\rangle$. Presume that states and observables in these two frames of reference are connected through the unitary frame transformation $U_{\text{RF}}(t)$. Specifically, states and observables are interconnected through the relationships $|\psi(t)\rangle = U_{\text{RF}}(t) |\psi_{\text{RF}}(t)\rangle$ and $O(t) = U_{\text{RF}}(t) O_{\text{RF}}(t) U_{\text{RF}}^\dagger(t)$, respectively [36]. To find $H_{\text{RF}}(t)$, we will proceed in the following manner. Observe that, $i\hbar\partial_t |\psi_{\text{RF}}(t)\rangle = H_{\text{RF}}(t) |\psi_{\text{RF}}(t)\rangle$ where

$$\begin{aligned} i\hbar\partial_t |\psi_{\text{RF}}(t)\rangle &= i\partial_t \left[U_{\text{RF}}^\dagger(t) |\psi(t)\rangle \right] \\ &= iU_{\text{RF}}^\dagger(t) \partial_t |\psi(t)\rangle + i \frac{\partial U_{\text{RF}}^\dagger(t)}{\partial t} |\psi(t)\rangle \\ &= iU_{\text{RF}}^\dagger(t) \left[\frac{1}{i} H(t) |\psi(t)\rangle \right] + i \frac{\partial U_{\text{RF}}^\dagger(t)}{\partial t} U_{\text{RF}}(t) |\psi_{\text{RF}}(t)\rangle \\ &= \left[U_{\text{RF}}^\dagger(t) H(t) U_{\text{RF}}(t) + i \frac{\partial U_{\text{RF}}^\dagger(t)}{\partial t} U_{\text{RF}}(t) \right] |\psi_{\text{RF}}(t)\rangle. \end{aligned} \quad (46)$$

Therefore, Eq. (46) yields

$$H_{\text{RF}}(t) = U_{\text{RF}}^\dagger(t) H(t) U_{\text{RF}}(t) + i \frac{\partial U_{\text{RF}}^\dagger(t)}{\partial t} U_{\text{RF}}(t). \quad (47)$$

Given that $U_{\text{RF}}^\dagger(t) U_{\text{RF}}(t) = U_{\text{RF}}(t) U_{\text{RF}}^\dagger(t) = \mathbf{1}$, Eq. (47) can be recast as

$$H_{\text{RF}}(t) = U_{\text{RF}}^\dagger(t) H(t) U_{\text{RF}}(t) - iU_{\text{RF}}^\dagger(t) \frac{\partial U_{\text{RF}}(t)}{\partial t}. \quad (48)$$

Given the expression of $H_{\text{RF}}(t)$ in Eq. (48), we can now introduce our illustrative example.

2. Illustrative example

In what follows, we study the evolution of a two-level quantum system which is initially in the state $|\psi(0)\rangle \stackrel{\text{def}}{=} |0\rangle$ and evolves under the time dependent Hamiltonian

$$H(t) \stackrel{\text{def}}{=} \frac{\hbar\omega}{2} [\cos(\nu t) \sigma_x + \sin(\nu t) \sigma_y]. \quad (49)$$

To clarify, it is important to mention that the quantum evolution defined by the Hamiltonian in Eq. (49) can be interpreted as an electron situated within a magnetic field arrangement, similar to that depicted in (c) of Fig. 2. Given this initial condition and the Hamiltonian in Eq. (49), one notices that $\mathbf{n}(t) = (\cos(\nu t), \sin(\nu t), 0)$ and $\mathbf{a}_0 = (0, 0, 1)$. Therefore, $\mathbf{n}(t) \cdot \mathbf{a}_0 = 0$ at any instant. However, as we shall see in this example, there exists no temporal instance t_* with $t_i \leq t_* \leq t_f$ for which $\mathcal{K}(t_*) = 1$ (unlike what happens in any stationary scenario). Obviously, t_i and t_f denote here the initial and final temporal instances, respectively. To verify the absence of such t_* , we need to evaluate Krylov's state complexity $\mathcal{K}(t) = 1 - |\langle\psi(0)|\psi(t)\rangle|^2$. We therefore need to find the evolving state $|\psi(t)\rangle$ under $H(t)$ in Eq. (49). To do so, we use the concept of rotating frame in quantum mechanics. To select the proper rotating frame that simplifies the integration of the Schrödinger equation, we note that

$$\cos(\nu t) \sigma_x + \sin(\nu t) \sigma_y = e^{-i\frac{\nu t}{2}\sigma_z} \sigma_x e^{i\frac{\nu t}{2}\sigma_z}. \quad (50)$$

As a consequence, it happens to be convenient to go into the rotating frame specified by the unitary $U_{\text{RF}}(t) = e^{-i\frac{\nu t}{2}\sigma_z}$. Substituting this specific expression of $U_{\text{RF}}(t)$ in $H_{\text{RF}}(t)$ in Eq. (48), we arrive at a time-independent expression for the Hamiltonian $H_{\text{RF}}(t)$ given by $H_{\text{RF}} = (1/2)(\omega\sigma_x - \nu\sigma_z)$. Having H_{RF} , we wish to solve the equation $i\partial_t|\psi_{\text{RF}}(t)\rangle = H_{\text{RF}}|\psi_{\text{RF}}(t)\rangle$. Then, given $|\psi_{\text{RF}}(t)\rangle$, we can find $|\psi(t)\rangle = U_{\text{RF}}(t)|\psi_{\text{RF}}(t)\rangle$ and $\mathcal{K}(t) = 1 - |\langle\psi(0)|\psi(t)\rangle|^2$. Note that $H_{\text{RF}} = (1/2)(\omega\sigma_x - \nu\sigma_z)$ can be recast as $H_{\text{RF}} = (\Omega/2)\mathbf{n} \cdot \boldsymbol{\sigma}$, where $\Omega \stackrel{\text{def}}{=} \sqrt{\omega^2 + \nu^2}$, and $\mathbf{n} \stackrel{\text{def}}{=} \frac{1}{\Omega}(\omega, 0, -\nu)$ with $\mathbf{n} \cdot \mathbf{n} = 1$. Then, setting the reduced Planck constant \hbar equal to one, we have

$$|\psi_{\text{RF}}(t)\rangle = e^{-iH_{\text{RF}}t}|0\rangle = \left[\cos\left(\frac{\Omega t}{2}\right) \mathbf{1} - i \sin\left(\frac{\Omega t}{2}\right) \mathbf{n} \cdot \boldsymbol{\sigma} \right] |0\rangle, \quad (51)$$

that is,

$$|\psi_{\text{RF}}(t)\rangle = \left[\cos\left(\frac{\Omega t}{2}\right) + i \frac{\nu}{\Omega} \sin\left(\frac{\Omega t}{2}\right) \right] |0\rangle - i \frac{\omega}{\Omega} \sin\left(\frac{\Omega t}{2}\right) |1\rangle. \quad (52)$$

From Eq. (52), we find

$$|\psi(t)\rangle = U_{\text{RF}}(t)|\psi_{\text{RF}}(t)\rangle = e^{-i\frac{\nu t}{2}\sigma_z} \left\{ \left[\cos\left(\frac{\Omega t}{2}\right) + i \frac{\nu}{\Omega} \sin\left(\frac{\Omega t}{2}\right) \right] |0\rangle - i \frac{\omega}{\Omega} \sin\left(\frac{\Omega t}{2}\right) |1\rangle \right\}, \quad (53)$$

that is,

$$|\psi(t)\rangle = \left[\cos\left(\frac{\Omega t}{2}\right) + i \frac{\nu}{\Omega} \sin\left(\frac{\Omega t}{2}\right) \right] e^{-i\frac{\nu t}{2}} |0\rangle - i \frac{\omega}{\Omega} \sin\left(\frac{\Omega t}{2}\right) e^{i\frac{\nu t}{2}} |1\rangle. \quad (54)$$

The interested reader can explicitly verify that $|\psi(t)\rangle$ in Eq. (54) solves $i\hbar\partial_t|\psi(t)\rangle = H(t)|\psi(t)\rangle$ with $H(t)$ in Eq. (49) once one sets $\hbar = 1$. Finally, using Eq. (54), $\mathcal{K}(t) = 1 - |\langle\psi(0)|\psi(t)\rangle|^2$ with $|\psi(0)\rangle = |0\rangle$ reduces to

$$\mathcal{K}(t) = \frac{\omega^2}{\omega^2 + \nu^2} \sin^2\left(\frac{\sqrt{\omega^2 + \nu^2}}{2}t\right). \quad (55)$$

From Eq. (55), we make several observations. Firstly, since $\sin^2(\xi t)$ is periodic of $T = \frac{1}{2} \cdot \frac{2\pi}{\xi} = \frac{\pi}{\xi} \equiv \frac{2\pi}{\omega_R}$, it oscillates with frequency $\omega_R = 2\xi$. Therefore, in our illustrative example, $\mathcal{K}(t)$ in Eq. (55) oscillates with frequency $\Omega = \sqrt{\omega^2 + \nu^2}$. Secondly, as $\nu \rightarrow 0$, $H \rightarrow \frac{\omega}{2}\sigma_x$. Then, $\mathcal{K}(t) = \sin^2(\frac{\omega}{2}t) \rightarrow 1$ as $t \rightarrow \frac{\pi}{\omega}$. For completeness, observe that $e^{-i\frac{\omega}{2}\sigma_x t}|0\rangle \stackrel{t=\frac{\pi}{\omega}}{=} e^{-i\frac{\pi}{2}\sigma_x}|0\rangle = -i|1\rangle \simeq |1\rangle$ (with “ \simeq ” denoting here physical equivalence of quantum states that differ by a global phase factor). Thirdly, the amplitude of $\mathcal{K}(t)$ is bounded by $\omega^2/(\omega^2 + \nu^2) < 1$, although $\mathbf{n}(t) \cdot \mathbf{a}_0 = 0$ at any instant. Therefore, we conclude that unlike what happens in any stationary scenario in which $\mathbf{n}(t) \cdot \mathbf{a}_0 = 0$ for any instant t (where the dynamical trajectory is a geodesic path on the Bloch sphere given by a fixed great circle), in our nonstationary scenario $|\psi(t)\rangle$ never gets fully orthogonal to $|\psi(0)\rangle$. After detailing these comments, we bring our discussion here a close.

Having outlined the fundamental aspects of Krylov's state complexity and our quantum IG complexity measure, and having reformulated Krylov's state complexity in geometric terms, we are now prepared to introduce our comparative analysis aimed at gaining insights rather than pursuing generality.

V. COMPARATIVE ASPECTS IN STATIONARY SCENARIOS

In this section, we perform a comparative analysis of these two complexity measures by explicitly investigating both geodesic and non-geodesic evolutions defined by time-independent Hamiltonians.

A. Geodesic motion

In this first scenario, we consider the evolution from the state $|\psi(t_i)\rangle = |0\rangle$ to the state $|\psi(t_f)\rangle = |+\rangle \stackrel{\text{def}}{=} (|0\rangle + |1\rangle)/\sqrt{2}$ under the time independent Hamiltonian $H \stackrel{\text{def}}{=} (1/\sqrt{6})\hbar\omega\sigma_y$. Clearly, t_i and t_f denote the initial and final times, respectively. We note that the quantum evolution characterized by the Hamiltonian H can be understood as an electron positioned within a configuration of a magnetic field, akin to that illustrated in (a) of Fig. 2.

Dynamics. From a simple calculation, we note that the evolved unit quantum state vector $|\psi(t)\rangle = e^{-\frac{i}{\hbar}Ht}|0\rangle$ with $t_i \leq t \leq t_f$ is given by

$$|\psi(t)\rangle = \cos\left(\frac{\omega t}{\sqrt{6}}\right)|0\rangle + \sin\left(\frac{\omega t}{\sqrt{6}}\right)|1\rangle. \quad (56)$$

From Eq. (56), we note that $|\psi(t_f)\rangle = |+\rangle$ if and only if $t_f = [\sqrt{6}\arccos(1/\sqrt{2})]/\omega = (\pi\sqrt{6})/(4\omega)$. Interestingly, t_f coincides with the shortest possible time t_{geo} needed to reach the state $|+\rangle$, when one starts in the state $|0\rangle$ with a Hamiltonian H with energy uncertainty $\Delta E \stackrel{\text{def}}{=} \sqrt{\langle 0|H^2|0\rangle - \langle 0|H|0\rangle^2} = \hbar\omega/\sqrt{6}$. Indeed, in these working conditions, t_{geo} becomes

$$t_{\text{geo}} \stackrel{\text{def}}{=} \frac{\hbar \arccos[|\langle 0|+\rangle|]}{\Delta E} = \frac{\sqrt{6}\arccos(1/\sqrt{2})}{\omega} = t_f. \quad (57)$$

Furthermore, it is straightforward to confirm that η_{GE} in Eq. (6) is equal to one for this quantum evolution.

To ensure thoroughness, we emphasize that our complexity measure C is independent of the orthonormal basis selected to represent the time-evolved quantum state of the system. In this document, we consistently express $|\psi(t)\rangle$ using the computational basis $\{|0\rangle, |1\rangle\}$. Nevertheless, this choice is not obligatory, and an alternative convenient basis may be utilized. It is important to note that while \bar{V} and V_{max} remain unaffected by the selection of this basis, the temporal variation of the instantaneous volume $V(t)$ may indeed be influenced by the specific basis chosen. In Fig. 6, we present a visual illustration that facilitates comprehension of the basis-independence inherent in our quantum IG complexity measure. Additional technical information regarding these aspects can be found in Appendix C for those interested.

Average Krylov complexity. We define the average Krylov complexity in the geodesic case as,

$$\langle \mathcal{K} \rangle_{\text{geo}} \stackrel{\text{def}}{=} \frac{1}{t_f - t_i} \int_{t_i}^{t_f} \mathcal{K}(t) dt, \quad (58)$$

where $\mathcal{K}(t) \stackrel{\text{def}}{=} \sum_{n=0}^1 n p_n(t)$ is the (instantaneous) Krylov complexity and, in addition, the probabilities $p_n(t)$ are specified

by $p_n(t) \stackrel{\text{def}}{=} |\langle \phi_n | \psi(t) \rangle|^2$ with $\{|\phi_n\rangle\}_{0 \leq n \leq 1}$ being an orthonormal Krylov basis. Applying the Gram-Schmidt orthonormalization procedure to the set $\{|0\rangle, H|0\rangle\}$, one arrives at $\{|\phi_n\rangle\}_{0 \leq n \leq 1} = \{|\phi_0\rangle, |\phi_1\rangle\} = \{|0\rangle, |1\rangle\}$. Therefore, a simple calculation yields $\mathcal{K}(t) = \sin^2(\omega t/\sqrt{6})$. Finally, $\langle \mathcal{K} \rangle_{\text{geo}}$ in Eq. (58) reduces to

$$\langle \mathcal{K} \rangle_{\text{geo}} = \frac{4\omega}{\pi\sqrt{6}} \int_0^{\frac{\pi\sqrt{6}}{4\omega}} \sin^2\left(\frac{\omega t}{\sqrt{6}}\right) dt = \frac{1}{2} - \frac{1}{\pi} \sim 0.181. \quad (59)$$

The quantity $\langle \mathcal{K} \rangle_{\text{geo}}$ in Eq. (59) represents the average Krylov complexity of the geodesic evolution from the state $|0\rangle$ to the state $|+\rangle$ under the Hamiltonian $H \stackrel{\text{def}}{=} (1/\sqrt{6})\hbar\omega\sigma_y$.

Quantum IGC. In the scenario being considered, the polar and azimuthal angles that specify the Bloch representation of the state $|\psi(t)\rangle$ in Eq. (56) are given by $\theta(t) = 2\omega t/\sqrt{6}$ and $\varphi(t) = 0$, respectively, with $0 \leq t \leq (\pi\sqrt{6})/(4\omega)$. By means of simple calculations, we find that the instantaneous volume equals $V(t) \stackrel{\text{def}}{=} \int_{\theta(0)}^{\theta(t)} (1/2) d\theta = \omega t/\sqrt{6}$, the

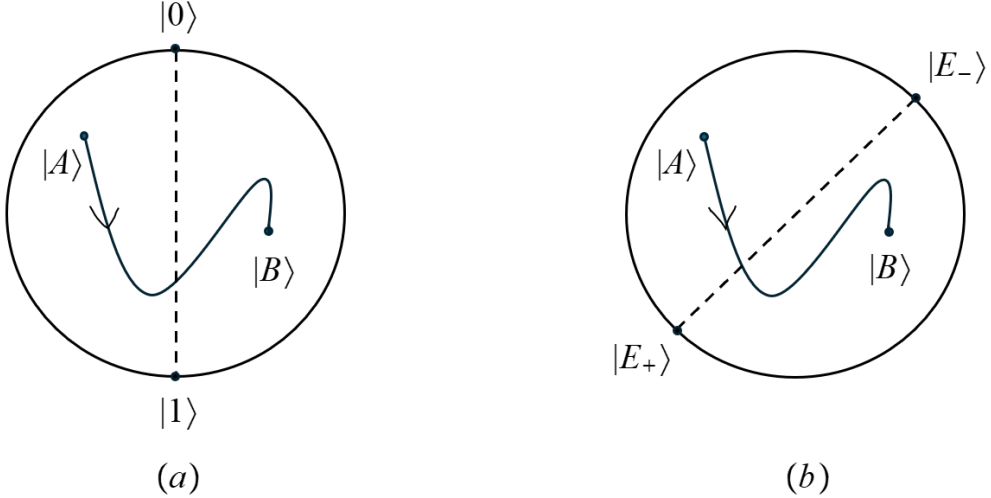


FIG. 6: Sketch to illustrate the basis-independence of our quantum IG complexity measure. The complexity $C(t_A, t_B)$ does not depend on the particular orthonormal basis chosen to decompose the energy state $|\psi(t)\rangle = \langle 0|\psi(t)\rangle|0\rangle + \langle 1|\psi(t)\rangle|1\rangle = \langle E_-|\psi(t)\rangle|E_-\rangle + \langle E_+|\psi(t)\rangle|E_+\rangle$. Although the parametrizations of the quantum amplitudes with spherical angles can differ in different bases, the accessed (i.e., \bar{V}) and accessible (i.e., V_{\max}) volumes used to construct the complexity measure do not change. Here, $\{|0\rangle, |1\rangle\}$ denotes the computational basis, while $\{|E_-\rangle, |E_+\rangle\}$ is the basis determined by eigenstates of the Hamiltonian of the system. Finally, $|A\rangle \stackrel{\text{def}}{=} |\psi(t_A)\rangle$ and $|B\rangle \stackrel{\text{def}}{=} |\psi(t_B)\rangle$ are the initial and final states, respectively.

accessible volume is given by $\bar{V} \stackrel{\text{def}}{=} (t_f - t_i)^{-1} \int_{t_i}^{t_f} V(t) dt = \pi/8$ (regardless of the chosen value of ω) and, lastly, the accessible volume is $V_{\max} \stackrel{\text{def}}{=} \int_{\theta_{\min}}^{\theta_{\max}} (1/2) d\theta = \pi/4$ with $\theta_{\min} = 0$ and $\theta_{\max} = \pi/2$. Therefore, the quantum IGC becomes

$$C_{\text{geo}} \stackrel{\text{def}}{=} \frac{V_{\max} - \bar{V}}{V_{\max}} = \frac{1}{2} = 0.5. \quad (60)$$

The quantity C_{geo} in Eq. (60) denotes the quantum IGC of the geodesic evolution from the state $|0\rangle$ to the state $|+\rangle$ under the Hamiltonian $H \stackrel{\text{def}}{=} (1/\sqrt{6})\hbar\omega\sigma_y$. We emphasize that our quantum IG measure of complexity is independent of the basis selected for decomposing the time-evolving state $|\psi(t)\rangle$. For further information, the interested reader may refer to Appendix C.

For completeness, we emphasize the time-dependent Bloch vector is given by

$$\mathbf{a}_{\text{geo}}(t) = \left(\sin\left(\frac{2\omega t}{\sqrt{6}}\right), 0, \cos\left(\frac{2\omega t}{\sqrt{6}}\right) \right), \quad (61)$$

with $\mathbf{a}_{\text{geo}}(t_i) = (0, 0, 1) \leftrightarrow |0\rangle$ and $\mathbf{a}_{\text{geo}}(t_f) = (1, 0, 0) \leftrightarrow |+\rangle$. Let \mathbf{n} be the unit vector that specifies the ‘‘magnetic field vector’’ $\mathbf{h} \stackrel{\text{def}}{=} h\mathbf{n}$ that enters the Hamiltonian $H = \mathbf{h} \cdot \boldsymbol{\sigma}$ with $h \stackrel{\text{def}}{=} \|\mathbf{h}\| = (1/\sqrt{6})\hbar\omega$. Since $\mathbf{a}_{\text{geo}}(t_i)$ is orthogonal to $\mathbf{n} = (0, 1, 0)$, we have that this geodesic evolution is characterized by a maximal ‘‘instantaneous’’ Krylov state complexity given by $\mathcal{K}(t) = \sin^2(\omega t/\sqrt{6})$. Moreover, from Eq. (10), we note that the curvature coefficient κ_{AC}^2 of this quantum evolution is zero.

From $\mathbf{a}(t) = \left(\sin\left(\frac{2\omega t}{\sqrt{6}}\right), 0, \cos\left(\frac{2\omega t}{\sqrt{6}}\right) \right)$ and $\mathbf{a}(0) = (0, 0, 1)$, we have $\|\mathbf{a}(t) - \mathbf{a}(0)\|^2 = 4 \sin^2\left(\frac{\omega t}{\sqrt{6}}\right) = 4\mathcal{K}(t)$. Therefore, since $\mathcal{K}(t) \propto \|\mathbf{a}(t) - \mathbf{a}(0)\|^2$, the square root of Krylov’s state complexity can be regarded as a measure of the distance between the initial Bloch vector $\mathbf{a}(0)$ and the time-evolved Bloch vector $\mathbf{a}(t)$ at a later time t . We also note that near $t = 0$, $\mathcal{K}(t) \leq C_{\mathcal{B}}(t)$, with \mathcal{B} being an ordered, complete, and orthonormal basis for the Krylov subspace defined in terms of the eigenvectors of the Hamiltonian $H \stackrel{\text{def}}{=} \frac{\hbar\omega}{\sqrt{6}}\sigma_y$. Indeed, σ_y has eigenvalues $\lambda_- \stackrel{\text{def}}{=} -1$ and $\lambda_+ \stackrel{\text{def}}{=} +1$, with corresponding eigenspaces $\mathcal{E}_{\lambda_-} \stackrel{\text{def}}{=} \text{Span}\{|E_-\rangle\}$ and $\mathcal{E}_{\lambda_+} \stackrel{\text{def}}{=} \text{Span}\{|E_+\rangle\}$. In our case, the orthonormal eigenstates $|E_-\rangle$ and $|E_+\rangle$ are given by

$$|E_-\rangle \stackrel{\text{def}}{=} \frac{|0\rangle - i|1\rangle}{\sqrt{2}}, \text{ and } |E_+\rangle \stackrel{\text{def}}{=} \frac{|0\rangle + i|1\rangle}{\sqrt{2}}, \quad (62)$$

respectively. More explicitly, we get $\mathcal{K}(t) = \sin^2(\frac{\omega t}{\sqrt{6}}) \leq \frac{1}{2} = |\langle E_+ | \psi(t) \rangle|^2 = C_B(t)$ for any $0 \leq t \leq \frac{\pi\sqrt{6}}{4\omega}$. For completeness, we stress that $|\langle E_- | \psi(t) \rangle|^2 = \frac{1}{2}$ and, as expected, $|\langle E_+ | \psi(t) \rangle|^2 + |\langle E_- | \psi(t) \rangle|^2 = 1$. For additional information regarding the relationships between $\mathcal{K}(t)$, $\|\mathbf{a}(t) - \mathbf{a}(0)\|^2$, and the Fubini-Study finite volume element $V_{\text{FS}}(t)$, we recommend referring to Appendix D.

B. Nongeodesic motion

In this second scenario, we consider the evolution from the state $|\psi(t_i)\rangle = |0\rangle$ to the state $|\psi(t_f)\rangle = |+\rangle \stackrel{\text{def}}{=} (|0\rangle + |1\rangle)/\sqrt{2}$ under the time independent Hamiltonian $H \stackrel{\text{def}}{=} (\hbar\omega/2)\mathbf{n} \cdot \boldsymbol{\sigma}$ with $\mathbf{n} \stackrel{\text{def}}{=} (1/\sqrt{3})(1, 1, 1)$ and $\boldsymbol{\sigma} \stackrel{\text{def}}{=} (\sigma_x, \sigma_y, \sigma_z)$. For completeness, we observe that the initial and final states in both geodesic and nongeodesic evolutions are the same. This is obviously required to have a fair comparison between the different types of evolutions. We also observe that the quantum evolution defined by the Hamiltonian H can be interpreted as an electron situated within a magnetic field configuration, similar to that depicted in (a) of Fig. 2.

Dynamics. From a straightforward calculation, we observe that the evolved unit quantum state vector $|\psi(t)\rangle = e^{-\frac{\hbar}{\hbar}Ht}|0\rangle$ with $t_i \leq t \leq t_f$ reduces to

$$|\psi(t)\rangle = \left[\cos\left(\frac{\omega t}{2}\right) - i\frac{1}{\sqrt{3}}\sin\left(\frac{\omega t}{2}\right) \right] |0\rangle - i\frac{1+i}{\sqrt{3}}\sin\left(\frac{\omega t}{2}\right) |1\rangle. \quad (63)$$

From Eq. (63), we note that $|\psi(t_f)\rangle$ is physically equivalent to $|+\rangle$ (i.e., $|\psi(t_f)\rangle = e^{i\phi}|+\rangle$ for some phase $\phi \in \mathbb{R}$) if and only if

$$\frac{-i\frac{1+i}{\sqrt{3}}\sin\left(\frac{\omega t_f}{2}\right)}{\cos\left(\frac{\omega t_f}{2}\right) - i\frac{1}{\sqrt{3}}\sin\left(\frac{\omega t_f}{2}\right)} = 1, \quad (64)$$

that is, if and only if $t_f = (2\pi)/(3\omega)$. Observe that $t_f^{\text{geo}} \stackrel{\text{def}}{=} (\pi\sqrt{6})/(4\omega) \sim 1.92/\omega \leq 2.09/\omega \sim (2\pi)/(3\omega) \stackrel{\text{def}}{=} t_f^{\text{nongeo}}$. We also notice that the comparison between $H \stackrel{\text{def}}{=} (1/\sqrt{6})\hbar\omega\sigma_y$ and $H \stackrel{\text{def}}{=} [(\hbar\omega)/(2\sqrt{3})](\sigma_x + \sigma_y + \sigma_z)$ is fair since the energy uncertainty of both Hamiltonians with respect to the initial state $|0\rangle$ assumes the same identical value of $\Delta E = \hbar\omega/\sqrt{6}$. Furthermore, it is simple to verify that η_{GE} in Eq. (6) is strictly less than one for this quantum evolution, since $\eta_{\text{GE}} = (3\sqrt{6})/8 \simeq 0.92 < 1$.

Average Krylov complexity. In this case, following the reasoning outlined for the geodesic evolution scenario, an easy calculation leads to $\mathcal{K}(t) = (2/3)\sin^2(\omega t/2)$. Therefore, the average Krylov complexity as given in Eq. (58) becomes

$$\langle \mathcal{K} \rangle_{\text{nongeo}} = \frac{3\omega}{2\pi} \int_0^{\frac{2\pi}{3\omega}} \frac{2}{3} \sin^2\left(\frac{\omega t}{2}\right) dt = \frac{1}{3} - \frac{\sqrt{3}}{4} \frac{1}{\pi} \sim 0.195. \quad (65)$$

The quantity $\langle \mathcal{K} \rangle_{\text{nongeo}}$ in Eq. (65) is the average Krylov complexity of the geodesic evolution from the state $|0\rangle$ to the state $|+\rangle$ under the Hamiltonian $H \stackrel{\text{def}}{=} [(\hbar\omega)/(2\sqrt{3})](\sigma_x + \sigma_y + \sigma_z)$. Comparing Eqs. (59) and (65), we note that $\langle \mathcal{K} \rangle_{\text{nongeo}} \geq \langle \mathcal{K} \rangle_{\text{geo}}$.

Quantum IGC. In the scenario being considered, we need to find the polar and azimuthal angles that specify the Bloch representation of the state $|\psi(t)\rangle$ in Eq. (63), where

$$|\psi(t)\rangle = a(t)|0\rangle + b(t)|1\rangle = \cos\left[\frac{\theta(t)}{2}\right]|0\rangle + e^{i\varphi(t)}\sin\left[\frac{\theta(t)}{2}\right]|1\rangle, \quad (66)$$

with $\theta(t) = 2\arccos[|a(t)|]$, $\varphi(t) = \arg[b(t)] - \arg[a(t)]$, with complex probability amplitudes $a(t)$ and $b(t)$ such that $|a(t)|^2 + |b(t)|^2 = 1$. After some algebraic manipulations, we arrive at an expression for the polar angle given by

$$\theta(t) = 2\arccos\left[\sqrt{1 - \frac{2}{3}\sin^2\left(\frac{\omega t}{2}\right)}\right], \quad (67)$$

with $\theta(0) = 0$ and $\theta(\frac{2\pi}{3\omega}) = \pi/2$. Moreover, the azimuthal angle becomes

$$\varphi(t) = -\frac{\pi}{4} + \arctan\left[\frac{1}{\sqrt{3}} \tan\left(\frac{\omega t}{2}\right)\right], \quad (68)$$

with $\varphi(0) = -\frac{\pi}{4}$ and $\varphi(\frac{2\pi}{3\omega}) = 0$. In this nongeodesic scenario, the instantaneous volume $V(t)$ is equal to

$$\begin{aligned} V(t) &= \frac{1}{4} \left| \left(\int_{\theta(0)}^{\theta(t)} \sin(\theta) d\theta \right) \left(\int_{\varphi(0)}^{\varphi(t)} d\varphi \right) \right| \\ &= \frac{1}{4} \left| \left\{ 1 - \cos \left[2 \arccos \left(\sqrt{1 - \frac{2}{3} \sin^2(\frac{\omega t}{2})} \right) \right] \right\} \arctan \left[\frac{1}{\sqrt{3}} \tan\left(\frac{\omega t}{2}\right) \right] \right|. \end{aligned} \quad (69)$$

The accessible volume defined as $\bar{V} \stackrel{\text{def}}{=} (t_f - t_i)^{-1} \int_{t_i}^{t_f} V(t) dt$ can be estimated numerically using Eq. (69), once one sets $t_i = 0$ and $t_f = (2\pi)/(3\omega)$. We have, $\bar{V} \sim 5.11 \times 10^{-2}$, irrespective of the specific value of ω . Finally, the accessible volume is

$$V_{\max} = \frac{1}{4} \left(\int_{\theta_{\min}}^{\theta_{\max}} \sin(\theta) d\theta \right) \left(\int_{\varphi_{\min}}^{\varphi_{\max}} d\varphi \right) = \frac{\pi}{16}, \quad (70)$$

where $\theta_{\min} = 0$, $\theta_{\max} = \pi/2$, $\varphi_{\min} = -\pi/4$, and $\varphi_{\max} = 0$. Therefore, the quantum IGC reduces to

$$C_{\text{nongeo}} \stackrel{\text{def}}{=} \frac{V_{\max} - \bar{V}}{V_{\max}} \sim 0.74. \quad (71)$$

The quantity C_{nongeo} in Eq. (71) specifies the quantum IGC of the nongeodesic evolution from the state $|0\rangle$ to the state $|+\rangle$ under the Hamiltonian $H \stackrel{\text{def}}{=} [(\hbar\omega)/(2\sqrt{3})] (\sigma_x + \sigma_y + \sigma_z)$. Comparing Eqs. (60) and (71), we conclude that $C_{\text{nongeo}} \geq C_{\text{geo}}$.

For completeness, we remark the time-dependent Bloch vector is given by

$$\mathbf{a}_{\text{nongeo}}(t) = (\sin(\theta_t) \cos(\varphi_t), \sin(\theta_t) \sin(\varphi_t), \cos(\theta_t)), \quad (72)$$

where $\theta_t = \theta(t)$ in Eq. (67) and $\varphi_t = \varphi(t)$ in Eq. (68). Lastly, observe that $\mathbf{a}_{\text{nongeo}}(t_i) = (0, 0, 1) \leftrightarrow |0\rangle$ and $\mathbf{a}_{\text{nongeo}}(t_f) = (1, 0, 0) \leftrightarrow |+\rangle$. Since $\mathbf{a}_{\text{nongeo}}(t_i)$ is not orthogonal to $\mathbf{n} = (1/\sqrt{3})(1, 1, 1)$ (i.e., the unit vector that specifies the “magnetic field vector” $\mathbf{h} \stackrel{\text{def}}{=} h\mathbf{n}$ that enters the Hamiltonian $H = \mathbf{h} \cdot \boldsymbol{\sigma}$ with $h \stackrel{\text{def}}{=} \|\mathbf{h}\| = (\hbar\omega)/2$), we have that this nongeodesic evolution is not characterized by a maximal “instantaneous” Krylov state complexity given that $\mathcal{K}(t) = (2/3) \sin^2(\omega t/2) \leq \sin^2(\omega t/2)$.

From $\mathbf{a}(t) = (\sin(\theta_t) \cos(\varphi_t), \sin(\theta_t) \sin(\varphi_t), \cos(\theta_t))$ and $\mathbf{a}(0) = (0, 0, 1)$, we obtain $\|\mathbf{a}(t) - \mathbf{a}(0)\|^2 = 4 \sin^2(\frac{\theta_t}{2})$. Given that $\theta_t = 2 \arccos(\sqrt{1 - \frac{2}{3} \sin^2(\frac{\omega t}{2})})$ and $\sin^2(\arccos(x)) = 1 - x^2$, we arrive at $\|\mathbf{a}(t) - \mathbf{a}(0)\|^2 = \frac{8}{3} \sin^2(\frac{\omega t}{2}) = 4\mathcal{K}(t)$. Consequently, given that $\mathcal{K}(t) \propto \|\mathbf{a}(t) - \mathbf{a}(0)\|^2$, the square root of Krylov’s state complexity can be interpreted as an indicator of the distance separating the initial Bloch vector $\mathbf{a}(0)$ from the time-evolved Bloch vector $\mathbf{a}(t)$ at a subsequent time t . Furthermore, we notice that the curvature coefficient κ_{AC}^2 of this quantum evolution is different from zero since one can check that $\kappa_{\text{AC}}^2 = 2 \neq 0$. We also observe that near $t = 0$, $\mathcal{K}(t) \leq C_{\mathcal{B}}(t)$, with \mathcal{B} being an ordered, complete, and orthonormal basis for the Krylov subspace defined by means of the eigenvectors of the Hamiltonian $H \stackrel{\text{def}}{=} \frac{\hbar\omega}{2} \frac{\sigma_x + \sigma_y + \sigma_z}{\sqrt{3}}$. Indeed, $\frac{\sigma_x + \sigma_y + \sigma_z}{\sqrt{3}}$ possesses eigenvalues $\lambda_- \stackrel{\text{def}}{=} -1$ and $\lambda_+ \stackrel{\text{def}}{=} +1$, with corresponding eigenspaces $\mathcal{E}_{\lambda_-} \stackrel{\text{def}}{=} \text{Span}\{|E_-\rangle\}$ and $\mathcal{E}_{\lambda_+} \stackrel{\text{def}}{=} \text{Span}\{|E_+\rangle\}$. In our case, the orthonormal eigenstates $|E_-\rangle$ and $|E_+\rangle$ are given by

$$|E_-\rangle \stackrel{\text{def}}{=} \frac{1}{\sqrt{3 - \sqrt{3}}} \begin{pmatrix} -(1-i)\frac{\sqrt{3}}{3+\sqrt{3}} \\ 1 \end{pmatrix}, \text{ and } |E_+\rangle \stackrel{\text{def}}{=} \frac{1}{\sqrt{\frac{6}{3-\sqrt{3}}}} \begin{pmatrix} (1-i)\frac{\sqrt{3}}{3-\sqrt{3}} \\ 1 \end{pmatrix}, \quad (73)$$

respectively. More explicitly, we get $\mathcal{K}(t) = \frac{2}{3} \sin^2(\frac{\omega t}{2}) \leq \frac{3-\sqrt{3}}{12-6\sqrt{3}} = |\langle E_+ | \psi(t) \rangle|^2 = C_{\mathcal{B}}(t)$ for any t . For completeness, we remark that $|\langle E_- | \psi(t) \rangle|^2 = \frac{1}{3+\sqrt{3}}$ and, as expected, $|\langle E_+ | \psi(t) \rangle|^2 + |\langle E_- | \psi(t) \rangle|^2 = 1$.

After conducting a comparative analysis of these two complexity measures by examining both geodesic and nongeodesic evolutions defined by stationary Hamiltonians, we are now prepared to move on to nonstationary Hamiltonian models.

VI. COMPARATIVE ASPECTS IN NONSTATIONARY SCENARIOS

In this section, we conduct a comparative analysis of these two complexity measures by explicitly examining both geodesic and non-geodesic evolutions as defined by time-dependent Hamiltonians.

A. Hamiltonian model

In this subsection, we introduce a two-parameter family of time-varying Hamiltonians, which we aim to examine from a geometric viewpoint. Specifically, our focus is on the time-dependent configurations of the magnetic fields that define the Hamiltonians. We also will examine the temporal dynamics of the phase that governs the relative phase factor involved in the Bloch sphere decomposition of the evolving state by means of the computational basis state vectors.

In Ref. [22], a comprehensive Hermitian nonstationary qubit Hamiltonian $H(t)$ is developed in a way that it produces the identical motion $\pi(|\psi(t)\rangle)$ within the complex projective Hilbert space $\mathbb{C}P^1$ (or, correspondingly, on the Bloch sphere $S^2 \cong \mathbb{C}P^1$) as $|\psi(t)\rangle$, where the projection operator π is defined such that $\pi : \mathcal{H}_2^1 \ni |\psi(t)\rangle \mapsto \pi(|\psi(t)\rangle) \in \mathbb{C}P^1$. In general, it can be demonstrated that $H(t)$ can be expressed as

$$H(t) = iE|\partial_t m(t)\rangle\langle m(t)| - iE|m(t)\rangle\langle\partial_t m(t)|, \quad (74)$$

where, for the sake of simplicity, we define $|m(t)\rangle = |m\rangle$, $|\partial_t m(t)\rangle = |\dot{m}\rangle$, $E = 1$ and, finally, $\hbar = 1$. The unit state vector $|m\rangle$ satisfies the equations $\pi(|m(t)\rangle) = \pi(|\psi(t)\rangle)$ and $i\partial_t|m(t)\rangle = H(t)|m(t)\rangle$. The equation $\pi(|m(t)\rangle) = \pi(|\psi(t)\rangle)$ leads us to conclude that $|m(t)\rangle = c(t)|\psi(t)\rangle$, with $c(t)$ denoting a complex function. By stating that $\langle m|m \rangle = 1$, we infer that $|c(t)| = 1$. This condition indicates, therefore, that $c(t) = e^{i\phi(t)}$ for a particular real-valued phase $\phi(t)$. Subsequently, by applying the parallel transport condition $\langle m|\dot{m} \rangle = \langle \dot{m}|m \rangle = 0$, the phase $\phi(t)$ is determined as $i \int \langle \psi | \dot{\psi} \rangle dt$. Consequently, $|m(t)\rangle = \exp(-\int_0^t \langle \psi(t') | \partial_{t'} \psi(t') \rangle dt') |\psi(t)\rangle$. It is essential to emphasize that $H(t)$ in Eq. (74) is inherently traceless, as it consists exclusively of off-diagonal elements relative to the orthogonal basis $\{|m\rangle, |\partial_t m\rangle\}$. Furthermore, $H(t)$ represents a linear combination of traceless Pauli spin matrices. Finally, the condition $i\partial_t|m(t)\rangle = H(t)|m(t)\rangle$ indicates that $|m(t)\rangle$ adheres to the Schrödinger evolution equation. As a supplementary note, we wish to highlight that the unitary time propagator $U(t) = \mathcal{T} \exp(-i \int_0^t H(s) ds)$, which is associated with the Hamiltonian $H(t)$ in Eq. (74), can be represented as a path-ordered $SU(2; \mathbb{C})$ rotation, formulated as

$$U(t) = \mathcal{T} \exp\left(-\frac{i}{\hbar} \frac{E}{2} \int_0^t \{[\mathbf{a}(t') \times \dot{\mathbf{a}}(t')] \cdot \boldsymbol{\sigma}\} dt'\right), \quad (75)$$

where \mathcal{T} denotes the time-ordering operator. In fact, by defining the projection operator $P(t) \stackrel{\text{def}}{=} |m(t)\rangle\langle m(t)| = [\mathbf{1} + \mathbf{a}(t) \cdot \boldsymbol{\sigma}] / 2$ and utilizing the standard properties of Pauli matrices, one can derive the Hamiltonian expression $H(t) = iE[\dot{P}(t), P(t)] = (E/2)[\mathbf{a}(t) \times \dot{\mathbf{a}}(t)] \cdot \boldsymbol{\sigma}$, which is characterized by a “magnetic” field proportional to $\mathbf{a}(t) \times \dot{\mathbf{a}}(t)$ which is orthogonal to the Bloch vector $\mathbf{a}(t)$. After providing some critical preliminary information regarding Uzdin’s research in Ref. [22], we are now ready to present our proposed time-dependent Hamiltonian.

To commence, let us examine the normalized state vector $|\psi(t)\rangle$ defined as,

$$|\psi(t)\rangle \stackrel{\text{def}}{=} \cos[\alpha(t)]|0\rangle + e^{i\beta(t)} \sin[\alpha(t)]|1\rangle, \quad (76)$$

where $\alpha(t)$ and $\beta(t)$ are two generally time-dependent real-valued parameters. From Eq. (76), we observe that $\langle \psi(t) | \dot{\psi}(t) \rangle = i\dot{\beta}(t) \sin^2[\alpha(t)] \neq 0$. Consequently, let us determine $|m(t)\rangle = e^{-i\phi(t)}|\psi(t)\rangle$, with $\langle m(t)|\dot{m}(t)\rangle = 0$. We note that $\langle m(t)|\dot{m}(t)\rangle = 0$ if and only if $\dot{\phi}(t) = -i\langle \psi(t) | \dot{\psi}(t) \rangle = \dot{\beta}(t) \sin^2[\alpha(t)]$, which implies

$$\phi(t) = \int_0^t \dot{\beta}(t') \sin^2[\alpha(t')] dt'. \quad (77)$$

Given $|\psi(t)\rangle$ and $\phi(t)$ as defined in Eqs. (76) and (77), the state $|m(t)\rangle$ can be expressed as

$$|m(t)\rangle = e^{-i \int_0^t \dot{\beta}(t') \sin^2[\alpha(t')] dt'} \left\{ \cos[\alpha(t)]|0\rangle + e^{i\beta(t)} \sin[\alpha(t)]|1\rangle \right\}, \quad (78)$$

By setting $|m\rangle\langle m| = (1/2)(\mathbf{1} + \mathbf{a} \cdot \boldsymbol{\sigma})$, the application of Eq. (78) results in the formulation of the Bloch vector $\mathbf{a}(t)$ in relation to the real-valued time-dependent parameters $\alpha(t)$ and $\beta(t)$,

$$\mathbf{a} \stackrel{\text{def}}{=} \begin{pmatrix} a_x \\ a_y \\ a_z \end{pmatrix} = \begin{pmatrix} \sin(2\alpha) \cos(\beta) \\ \sin(2\alpha) \sin(\beta) \\ \cos(2\alpha) \end{pmatrix}. \quad (79)$$

From Eq. (79), we observe that $\mathbf{a} \cdot \mathbf{a} = a_x^2 + a_y^2 + a_z^2 = 1$. Finally, to derive the expression of $H(t) = i|\partial_t m(t)\rangle\langle m(t)| - i|m(t)\rangle\langle\partial_t m(t)|$ reformulated as $h_0(t)\mathbf{1} + \mathbf{h}(t) \cdot \boldsymbol{\sigma}$, it is necessary to determine the explicit formulas for both $h_0(t)$ and the magnetic field vector $\mathbf{h}(t)$. Through a series of algebraic manipulations, we reach the conclusion that

$$\begin{aligned} H(t) &= \begin{pmatrix} h_0 + h_z & h_x - ih_y \\ h_x + ih_y & h_0 - h_z \end{pmatrix} \\ &= \begin{pmatrix} 2\dot{\phi} \cos^2(\alpha) & e^{-i\beta} [2\dot{\phi} \sin(\alpha) \cos(\alpha) - i\dot{\alpha} - \dot{\beta} \sin(\alpha) \cos(\alpha)] \\ e^{i\beta} [2\dot{\phi} \sin(\alpha) \cos(\alpha) + i\dot{\alpha} - \dot{\beta} \sin(\alpha) \cos(\alpha)] & 2\dot{\phi} \sin^2(\alpha) - 2\dot{\beta} \sin^2(\alpha) \end{pmatrix}. \end{aligned} \quad (80)$$

From Eq. (80), we conclude that $h_0(t) = 0$ (as anticipated, given that the Hamiltonian is traceless). Furthermore, by utilizing Eq. (77), we observe from Eq. (80) that $\mathbf{h}(t)$ is equivalent to

$$\mathbf{h}(t) \stackrel{\text{def}}{=} \begin{pmatrix} h_x(t) \\ h_y(t) \\ h_z(t) \end{pmatrix} = \begin{pmatrix} -\frac{\dot{\beta}}{2} \cos(2\alpha) \sin(2\alpha) \cos(\beta) - \dot{\alpha} \sin(\beta) \\ -\frac{\dot{\beta}}{2} \cos(2\alpha) \sin(2\alpha) \sin(\beta) + \dot{\alpha} \cos(\beta) \\ \frac{\dot{\beta}}{2} \sin^2(2\alpha) \end{pmatrix}. \quad (81)$$

By utilizing Eqs. (79) and (81), one can confirm through straightforward yet tedious algebra that the Bloch vector and the magnetic vector satisfy the differential equation $\dot{\mathbf{a}} = 2\mathbf{h} \times \mathbf{a}$ [54]. Notably, it is observed that the Bloch vector $\mathbf{a}(t)$ in Eq. (79) and the magnetic field $\mathbf{h}(t)$ in Eq. (81) are orthogonal, as $\mathbf{a} \cdot \mathbf{h} = 0$ at all times. It is important to note that $\dot{\mathbf{a}} = 2\mathbf{h} \times \mathbf{a}$ indicated that $\dot{\mathbf{a}} \cdot \mathbf{h} = 0$. Consequently, since $\mathbf{a} \cdot \mathbf{h} = 0$ leads to $\dot{\mathbf{a}} \cdot \mathbf{h} + \mathbf{a} \cdot \dot{\mathbf{h}} = 0$, we also find that $\mathbf{a} \cdot \dot{\mathbf{h}} = 0$. In conclusion, we summarize the following relationships: (i) $\dot{\mathbf{a}} = 2\mathbf{h} \times \mathbf{a}$, which indicates $\dot{\mathbf{a}} \cdot \mathbf{h} = 0$; (ii) $\mathbf{a} \cdot \mathbf{h} = 0$, which leads to $\dot{\mathbf{a}} \cdot \mathbf{h} + \mathbf{a} \cdot \dot{\mathbf{h}} = 0$; (iii) $\mathbf{a} \cdot \dot{\mathbf{h}} = 0$, as a result of (i) and (ii). By utilizing the geometric constraints that exist between the Bloch and magnetic vectors, the curvature coefficient $\kappa_{\text{AC}}^2(\mathbf{a}, \mathbf{h})$ as presented in Eq. (9) simplifies to

$$\kappa_{\text{AC}}^2(\mathbf{h}) = \frac{(\mathbf{h}^2)(\dot{\mathbf{h}}^2) - (\mathbf{h} \cdot \dot{\mathbf{h}})^2}{\mathbf{h}^6}. \quad (82)$$

In the upcoming two subsections, we will focus on the time dependence of the previously discussed phase $\beta(t)$ to examine two distinct scenarios: i) no growth; ii) linear growth. These scenarios are characterized by specific magnetic field configurations $\mathbf{h}(t)$, which are affected by the generally time-varying real-valued parameters $\alpha(t)$ and $\beta(t)$. In particular, $\alpha(t)$ governs the time-dependent behavior of the quantum amplitudes of the evolving state $|\psi(t)\rangle$ in relation to the computational basis vectors $|0\rangle$ and $|1\rangle$, whereas $\beta(t)$ represents the quantum-mechanically observable relative phase factor that is incorporated into the expression of $|\psi(t)\rangle$. Our primary focus is on quantum evolutions that transition between orthogonal initial and final states $|A\rangle \stackrel{\text{def}}{=} |\psi(0)\rangle = |0\rangle$ and $|B\rangle \stackrel{\text{def}}{=} |\psi(t_f)\rangle \simeq |1\rangle$. Additionally, to emphasize the alterations in motion induced by various time-configurations of the relative phase factor defined by $\beta(t)$, we will establish $\alpha(t) \stackrel{\text{def}}{=} \omega_0 t$ with $\omega_0 \in \mathbb{R}_+ \setminus \{0\}$, throughout our comparative analysis. Based on the expression of $|\psi(t)\rangle$, this assumption regarding $\alpha(t)$ leads us to consider t_f as equal to $\pi/(2\omega_0)$.

B. Geodesic motion

In the first example, we consider that $\mathbf{h}(t)$ is defined by a phase $\beta(t)$ which remains constant over time. Specifically, we establish $\beta(t) \stackrel{\text{def}}{=} \beta_0 \in \mathbb{R}_+ \setminus \{0\}$ such that $\dot{\beta} = 0$. The evolution of interest transpires from $|A\rangle = |0\rangle$ to $|B\rangle \simeq |1\rangle$ within a time interval $t_f = \pi/(2\omega_0)$, keeping in mind our selection of $\alpha(t)$ as $\omega_0 t$. The symbol “ \simeq ” signifies the physical equivalence of quantum states, disregarding insignificant global phase factors.

Dynamics. From the perspective of geodesic efficiency, it is observed that the geodesic distance s_0 from $|A\rangle$ to $|B\rangle$ is given by $s_0 = \pi$. Additionally, the energy uncertainty $\Delta E(t) = \sqrt{\langle \dot{m} | \dot{m} \rangle}$ remains constant and is equal to

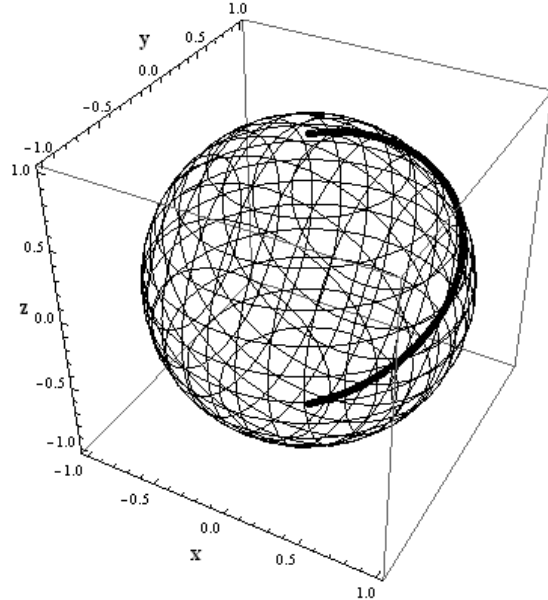


FIG. 7: An illustrative depiction of the geodesic evolution path (thick solid line) on the Bloch sphere, generated by the Hamiltonian evolution associated with $(\alpha(t), \beta(t)) \stackrel{\text{def}}{=} (\omega_0 t, \beta_0)$, where $0 \leq t \leq \pi/2$. The evolution shifts from $|A\rangle \stackrel{\text{def}}{=} |0\rangle$ to $|B\rangle \stackrel{\text{def}}{=} |1\rangle$. For simplicity, we set $\nu_0 = \omega_0 = 1$ and $\beta = \pi/4$. Physical units are chosen with $\hbar = 1$.

ω_0 , as $\langle \dot{m} | \dot{m} \rangle = \dot{\alpha}^2 + (1/4)\dot{\beta}^2 \sin^2(2\alpha)$. Consequently, this evolution occurs with a unit geodesic efficiency, $\eta_{\text{GE}} = 1$ since $s = s_0 = \pi$. The curvature coefficient κ_{AC}^2 in Eq. (82) pertaining to this quantum evolution is equal to zero. This aligns with the observation that the geodesic efficiency is one. From the perspective of a magnetic field, we have $\mathbf{h}^2 = \dot{\alpha}^2$, $\dot{\mathbf{h}}^2 = \ddot{\alpha}^2$, and $(\mathbf{h} \cdot \dot{\mathbf{h}})^2 = \dot{\alpha}^2 \ddot{\alpha}^2$. Consequently, the nullification of the curvature coefficient arises from the fact that $\mathbf{h}(t)$ and $\dot{\mathbf{h}}(t)$ are collinear (i.e., $\partial_t \hat{h}(t) = \mathbf{0}$, with $\mathbf{h}(t) = h(t)\hat{h}(t)$). In other terms, the magnetic field varies solely in intensity, while its direction remains unchanged. For the sake of thoroughness, we note that when $\beta(t) \stackrel{\text{def}}{=} \beta_0$, the temporal variation of $\alpha(t)$ does not have to be linear in t to achieve a geodesic evolution on the Bloch sphere. In fact, let us consider $\beta(t) \stackrel{\text{def}}{=} \beta_0$ and $\alpha(t) \stackrel{\text{def}}{=} \omega_0^2 t^2$. A simple calculation reveals that $\mathbf{h}(t) = \dot{\alpha}(t)(-\sin(\beta_0), \cos(\beta_0), 0)$ and $\dot{\mathbf{h}}(t) = \ddot{\alpha}(t)(-\sin(\beta_0), \cos(\beta_0), 0)$ so that $\mathbf{h}^2(t) = 4\omega_0^4 t^2$ with $\mathbf{h}(t)$ and $\dot{\mathbf{h}}(t)$ being collinear. Furthermore, after performing some algebraic manipulations, it can be confirmed that $\eta_{\text{GE}} = 2 \arccos(0) / (2 \int_0^{\frac{1}{\omega_0} \sqrt{\frac{\pi}{2}}} 2\omega_0^2 t dt) = 1$ and $\kappa_{\text{AC}}^2 = 0$. In conclusion, when $\beta(t) \stackrel{\text{def}}{=} \beta_0$, both $\alpha(t) \stackrel{\text{def}}{=} \omega_0 t$ and $\alpha(t) \stackrel{\text{def}}{=} \omega_0^2 t^2$ produce a great circle on the Bloch sphere. The distinction lies in the fact that in the first scenario, the evolution takes place at a constant speed. Conversely, in the second scenario, the speed of quantum evolution varies with time, as $v(t) \propto \Delta E(t) = \sqrt{\dot{\alpha}^2 + (1/4)\dot{\beta}^2 \sin^2(2\alpha)}$. We observe that the quantum evolution defined by the Hamiltonian H associated with $(\alpha(t), \beta(t)) = (\omega_0^2 t^2, \beta_0)$ can be interpreted as an electron within a magnetic field configuration, similar to that depicted in (b) of Fig. 2. In Fig. 7, we illustrate this geodesic quantum evolution.

Average Krylov complexity. Given that $|\psi(0)\rangle = |A\rangle = |0\rangle$ and

$$|\psi(t)\rangle_{\text{geo}} = \cos(\omega_0 t) |0\rangle + e^{i\beta_0} \sin(\omega_0 t) |1\rangle, \quad (83)$$

we have that $\mathcal{K}(t) = 1 - |\langle \psi(0) | \psi(t) \rangle|^2 = \sin^2(\omega_0 t)$. Therefore, the average Krylov state complexity in this geodesic scenario reduces to $\langle \mathcal{K} \rangle_{\text{geo}}$

$$\langle \mathcal{K} \rangle_{\text{geo}} = \frac{2\omega_0}{\pi} \int_0^{\frac{\pi}{2\omega_0}} \sin^2(\omega_0 t) dt = \frac{1}{2}. \quad (84)$$

Quantum IGC. Ultimately, from the perspective of quantum IGC, we find that $\theta(t) = 2\omega_0 t$ and $\varphi(t) = \beta_0$, with $0 \leq \theta \leq \pi$ and $0 \leq t \leq \pi/(2\omega_0)$. Consequently, a simple calculation provides the formulas for instantaneous, accessed, and accessible volumes $V(t) = \omega_0 t$, $\bar{V} = \pi/4$, and $V_{\text{max}} = \pi/2$, respectively. Thus, the quantum IGC of this quantum

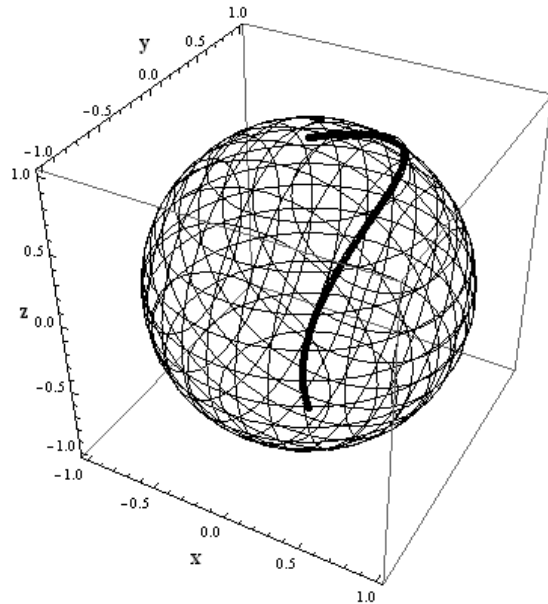


FIG. 8: An illustrative representation of the nongeodesic evolution trajectory (thick solid line) on the Bloch sphere, produced by the Hamiltonian evolution linked to $(\alpha(t), \beta(t)) \stackrel{\text{def}}{=} (\omega_0 t, \beta_0 + \nu_0 t)$, where $0 \leq t \leq \pi/2$. The evolution transitions from $|A\rangle \stackrel{\text{def}}{=} |0\rangle$ to $|B\rangle \stackrel{\text{def}}{=} |1\rangle$. For the sake of simplicity, we establish $\nu_0 = \omega_0 = 1$ and $\beta = \pi/4$. Physical units are selected with $\hbar = 1$.

evolution simplifies to

$$C_{\text{geo}} = \frac{V_{\text{max}} - \bar{V}}{V_{\text{max}}} = \frac{\frac{\pi}{2} - \frac{\pi}{4}}{\frac{\pi}{2}} = \frac{1}{2} \quad (85)$$

Interestingly, $\langle \mathcal{K} \rangle_{\text{geo}}$ in Eq. (84) and C_{geo} in Eq. (85) yield identical numerical values in this particular case.

C. Nongeodesic motion

In the second example, we assume that $\mathbf{h}(t)$ is defined by a phase $\beta(t)$ that increases linearly over time. Specifically, we express $\beta(t) \stackrel{\text{def}}{=} \beta_0 + \nu_0 t$, where $\beta_0, \nu_0 \in \mathbb{R}_+ \setminus \{0\}$, ensuring that $\dot{\beta} = \nu_0$. The evolution of focus occurs from $|A\rangle = |0\rangle$ to $|B\rangle \simeq |1\rangle$ within a time frame $t_f = \pi/(2\omega_0)$, once we recall our selection indicated by $\alpha(t) = \omega_0 t$. To ensure thoroughness, we note that the starting and ending states in both geodesic and non-geodesic evolutions are identical. This is clearly necessary for a just comparison among the various types of evolutions.

Dynamics. From the perspective of geodesic efficiency, we note that the geodesic distance s_0 from $|A\rangle$ to $|B\rangle$ is equal to $s_0 = \pi$. Furthermore, the energy uncertainty $\Delta E(t) = \sqrt{\langle \dot{m} | \dot{m} \rangle}$ is variable, as $\langle \dot{m} | \dot{m} \rangle = \dot{\alpha}^2 + (1/4)\dot{\beta}^2 \sin^2(2\alpha)$ leads to $\Delta E^2(t) = \omega_0^2 + (1/4)\nu_0^2 \sin^2(2\omega_0 t)$. Consequently, this evolution takes place with a geodesic efficiency that is not equal to one, $\eta_{\text{GE}} < 1$, since $s > s_0 = \pi$. Generally, the quantity η_{GE} depends on the parameters ω_0 and ν_0 and can be estimated numerically. For example, when $\omega_0 = \nu_0 = 1$, $s \simeq 3.33 \geq \pi = s_0$. We also note that the curvature coefficient κ_{AC}^2 in Eq. (82) of this quantum evolution is different from zero. This agrees with the fact that $\eta_{\text{GE}} < 1$. After some algebra, substituting Eq. (81) into Eq. (82) with $\alpha(t) \stackrel{\text{def}}{=} \omega_0 t$ and $\beta(t) \stackrel{\text{def}}{=} \beta_0 + \nu_0 t$, κ_{AC}^2 becomes

$$\kappa_{\text{AC}}^2(t; \omega_0, \nu_0) = \frac{\mathbf{h}^2(t; \omega_0, \nu_0) \dot{\mathbf{h}}^2(t; \omega_0, \nu_0) - [\mathbf{h}(t; \omega_0, \nu_0) \cdot \dot{\mathbf{h}}(t; \omega_0, \nu_0)]^2}{\mathbf{h}^6(t; \omega_0, \nu_0)}, \quad (86)$$

with \mathbf{h}^2 , $\dot{\mathbf{h}}^2$, and $(\mathbf{h} \cdot \dot{\mathbf{h}})^2$ in Eq. (86) being given by

$$\begin{aligned}\mathbf{h}^2 &\stackrel{\text{def}}{=} \frac{1}{8}\nu_0^2 + \omega_0^2 - \frac{1}{8}\nu_0^2 \cos(4\omega_0 t), \\ \dot{\mathbf{h}}^2 &\stackrel{\text{def}}{=} \frac{1}{32}\nu_0^4 - \frac{1}{32}\nu_0^4 \cos(8\omega_0 t) + 2\nu_0^2\omega_0^2 + 2\nu_0^2\omega_0^2 \cos(4\omega_0 t), \\ \mathbf{h} \cdot \dot{\mathbf{h}} &\stackrel{\text{def}}{=} \frac{1}{4}\nu_0^2\omega_0 \sin(4\omega_0 t),\end{aligned}\tag{87}$$

respectively. As a side remark, we note that the short-time limit of $\kappa_{\text{AC}}^2(t; \omega_0, \nu_0)$ is

$$\kappa_{\text{AC}}^2(t; \omega_0, \nu_0) \xrightarrow{t \rightarrow 0} 4\left(\frac{\nu_0}{\omega_0}\right)^2 - 8\left(\frac{\nu_0}{\omega_0}\right)^2(\nu_0^2 + 2\omega_0^2)t^2 + \mathcal{O}(t^3),\tag{88}$$

where $\kappa_{\text{AC}}^2(t; \omega_0, \nu_0)$ starts at the nonzero value of $4(\nu_0/\omega_0)^2$ at $t = 0$. Finally, the existence of a non-vanishing curvature coefficient arises from the fact that $\mathbf{h}(t)$ and $\dot{\mathbf{h}}(t)$ are not collinear (i.e., $\partial_t \hat{h}(t) \neq \mathbf{0}$, with $\mathbf{h}(t) = h(t)\hat{h}(t)$). Lastly, we remark that the quantum evolution specified by the Hamiltonian H specified by the pair $(\alpha(t), \beta(t)) = (\omega_0 t, \beta_0 + \nu_0 t)$ can be regarded as an electron immersed in a magnetic field configuration, similar to that illustrated in (d) of Fig. 2. In Fig. 8, we display the nongeodesic quantum-mechanical evolution path on the Bloch sphere.

Average Krylov complexity. Given that $|\psi(0)\rangle = |A\rangle = |0\rangle$ and

$$|\psi(t)\rangle_{\text{nongeo}} = \cos(\omega_0 t)|0\rangle + e^{i(\beta_0 + \nu_0 t)}\sin(\omega_0 t)|1\rangle,\tag{89}$$

we have that $\mathcal{K}(t) = 1 - |\langle\psi(0)|\psi(t)\rangle|^2 = \sin^2(\omega_0 t)$. Therefore, the average Krylov state complexity in this non-geodesic scenario reduces to $\langle\mathcal{K}\rangle_{\text{nongeo}}$

$$\langle\mathcal{K}\rangle_{\text{nongeo}} = \frac{2\omega_0}{\pi} \int_0^{\frac{\pi}{2\omega_0}} \sin^2(\omega_0 t) dt = \frac{1}{2}.\tag{90}$$

Interestingly, despite the fact that $|\psi(t)\rangle_{\text{geo}} \neq |\psi(t)\rangle_{\text{nongeo}}$, we have that $\langle\mathcal{K}\rangle_{\text{geo}}$ in Eq. (84) is equal to $\langle\mathcal{K}\rangle_{\text{nongeo}}$ in Eq. (90).

Quantum IGC. Ultimately, from the perspective of quantum IGC, we find that $\theta(t) = 2\omega_0 t$ and $\varphi(t) = \beta_0 + \nu_0 t$, with $0 \leq \theta \leq \pi$, $\beta_0 \leq \varphi \leq \beta_0 + (\pi/2)(\nu_0/\omega_0)$, and $0 \leq t \leq \pi/(2\omega_0)$. Consequently, a simple calculation provides the formulas for instantaneous, accessed, and accessible volumes

$$V(t) = \frac{\nu_0}{4} [1 - \cos(2\omega_0 t)] t, \quad \bar{V} = \left(\frac{1}{4\pi} + \frac{\pi}{16}\right) \frac{\nu_0}{\omega_0}, \quad \text{and} \quad V_{\text{max}} = \frac{\pi}{4} \frac{\nu_0}{\omega_0},\tag{91}$$

respectively. Thus, applying Eq. (91), the quantum IGC of this quantum evolution simplifies to

$$C_{\text{nongeo}} = \frac{V_{\text{max}} - \bar{V}}{V_{\text{max}}} = \frac{3\pi^2 - 4}{4\pi^2} \sim 0.65.\tag{92}$$

Interestingly, and in contrast to Krylov's state complexity, we observe that C_{nongeo} in Eq. (92) is approximately 0.65, which exceeds $C_{\text{geo}} = 1/2$. It is important to notice that in the scenario of linear growth, the quantum IGC in Eq. (92) attains a constant value that remains unaffected by the parameters ω_0 and ν_0 , stemming from the fact that both \bar{V} and V_{max} are proportional to the ratio (ν_0/ω_0) .

From our investigation, we note that the phase $\beta(t)$ alters the trajectory length from $|\psi(0)\rangle \stackrel{\text{def}}{=} |0\rangle$ to $|\psi(t_f)\rangle \stackrel{\text{def}}{=} |1\rangle$. Phase motion adds curvature to the path, increasing its length. However, as we have seen, a change in the path length does not imply a spread in the Krylov basis. Krylov's state complexity is blind to phase motion. It depends only on how far the state $|\psi(t)\rangle$ with $0 \leq t \leq t_f$ has traveled from the reference state $|0\rangle$ in a predetermined direction, rather than how it navigates around the Bloch sphere. This predetermined direction is represented by the orthonormal Krylov chain $\{|\phi_n\rangle\}_{n \geq 0}$, which is formed through the repeated application of the Hamiltonian on the reference state and constructed using Lanczos recursion. The unitary time evolution from the reference state is restricted to movement along this chain, and Krylov's state complexity corresponds to the anticipated position on that chain. In contrast to $\beta(t)$, which modifies the longitude by rotating the state around the z -axis, the parameter $\alpha(t)$ adjusts the latitude of the state, indicating the extent of transition from $|0\rangle$ to $|1\rangle$. Changes in $\beta(t)$ are identified exclusively by the quantum IGC, whereas variations in $\alpha(t)$ are acknowledged by both the quantum IGC and Krylov's state complexity.

We are now prepared to present our summary of results and final observations.

VII. FINAL REMARKS

In this paper, we conducted a comparative analysis of Krylov's state complexity $\mathcal{K}(t)$ (Eq. (16)) in conjunction with a quantum information geometric (IG) measure of complexity $C(t_A, t_B)$ with $t_A \leq t \leq t_B$ (Eq.(17)) that pertains to the quantum evolutions of two-level quantum systems. This analysis is based on geometric principles such as length, spread, and volumes, particularly concerning qubit dynamics on the Bloch sphere. In this context, the quantum mechanical evolutions are characterized by either stationary or nonstationary Hamiltonians, which can yield either geodesic (Eqs. (56) and (83)) or nongeodesic (Eqs. (54), (63), and (89)) dynamical trajectories. After presenting a geometric formulation of Krylov's state complexity in both its instantaneous and time-averaged forms, we applied the concepts of geodesic efficiency (i.e., η_{geo} in Eq. (6)) and curvature coefficient (i.e., κ_{AC}^2 in Eq. (9)) of quantum evolutions to extract physical insights into the various aspects represented by the two distinct measures of complexity. Ultimately, we illustrated that this differentiation is fundamentally due to the non-overlapping quantities utilized in the formulation of these measures, specifically the spread of the evolving quantum state in relation to a defined direction determined by the initial state, as well as the volume covered during the evolution on the Bloch sphere. Our primary findings can be summarized as follows:

- [i] We demonstrated that Krylov's state complexity can be expressed, in both stationary (Eqs. (33), (37), and (38)) and nonstationary (Eqs. (40) and (41)) contexts, utilizing vectors that have a unique geometric significance. In particular, we used Bloch vectors (i.e., \mathbf{a}_0 and \mathbf{a}_t) and magnetic field vectors (i.e., $\mathbf{h}(t)$), which define the Hamiltonians that govern the quantum mechanical evolutions.
- [ii] We illustrated that, in contrast to any stationary situation where $\mathbf{n}(t) \cdot \mathbf{a}_0 = 0$ for every moment t , with $H(t) \stackrel{\text{def}}{=} \mathbf{h}(t) \cdot \boldsymbol{\sigma}$, $\mathbf{h}(t) \stackrel{\text{def}}{=} h(t) \mathbf{n}(t)$, and $\rho(0) \stackrel{\text{def}}{=} |\psi(0)\rangle\langle\psi(0)| = [\mathbf{1} + \mathbf{a}_0 \cdot \boldsymbol{\sigma}] / 2$, and where the dynamic trajectory follows a geodesic path on the Bloch sphere defined by a constant great circle), in the nonstationary scenario we examined ($H(t)$ in Eq. (49)), $|\psi(t)\rangle$ does not become completely orthogonal to $|\psi(0)\rangle$. Consequently, there is no moment t at which $\mathcal{K}(t)$ reaches its maximum value of one (Eq. (55)).
- [iii] We showed that geodesic trajectories on the Bloch sphere, produced by stationary Hamiltonians, are typically defined by reduced levels of *time-averaged* Krylov state complexity (Eqs. (59) and (65)). Nevertheless, these geodesic evolutions not only proceed at a faster speed (i.e., as shorter travel time), but they also manifest with increased levels of *instantaneous* Krylov state complexity.
- [iv] We established that, similar to our quantum IG complexity measure, Krylov's state complexity exceeds mere length. In particular, by employing nonstationary Hamiltonian evolutions, we illustrated that different trajectories on the Bloch sphere that connect the same initial and final states can possess varying lengths while maintaining identical values of Krylov's state complexity (Eqs. (84) and (90)). Nevertheless, while $\mathcal{K}(t)$ is dependent on the idea of "spread", $C(t_A, t_B)$ (Eqs. (85) and (92)) is founded on the concept of "volume". Both spread and volume are distinct from the concept of length. Furthermore, we also confirmed, in stationary Hamiltonian contexts and for suitable temporal regimes, the relationships among $\mathcal{K}(t)$, $\|\mathbf{a}_t - \mathbf{a}_0\|^2$, and $V_{\text{FS}}(t)$ (Appendix D).
- [v] We verified that, in contrast to our quantum IG measure of complexity (85) and (92)), the existence of relative phases (i.e., $e^{i\beta(t)}$ in Eq. (76)) within quantum states $|\psi(t)\rangle$ does not affect the behavior of Krylov's state complexity $\mathcal{K}(t)$ (Eqs. (84) and (90)). The phase $\beta(t)$ modifies the trajectory length from $|\psi(0)\rangle \stackrel{\text{def}}{=} |0\rangle$ to $|\psi(t_f)\rangle \stackrel{\text{def}}{=} |1\rangle$. The motion of the phase introduces curvature to the path, thereby increasing its length. Nevertheless, an alteration in the path length does not signify a dispersion in the Krylov basis. Krylov's state complexity remains unaffected by phase motion. It is solely dependent on the distance the state $|\psi(t)\rangle$ with $0 \leq t \leq t_f$ has moved from the reference state $|0\rangle$ in a specified direction, rather than the manner in which it traverses the Bloch sphere.

Our research has two significant limitations. First, we have limited our analysis to quantum evolutions governed by Hamiltonians within the context of two-level quantum systems. Second, we have not explored the implications of our findings for understanding complexity in quantum-mechanical systems that are in mixed quantum states. Although it is theoretically possible to extend our study to arbitrary time-varying Hamiltonian evolutions, the computational challenge lies in obtaining accurate analytical solutions to the time-dependent Schrödinger equation for determining probability amplitudes. This task poses substantial difficulties, even in the domain of two-level quantum systems [52, 53, 55–64]. Furthermore, the transition from pure to mixed states presents various challenges, both computationally and conceptually. It is widely acknowledged that there exists an infinite variety of distinguishability metrics

applicable to mixed quantum states. This variety results in interpretations of essential geometric quantities, such as the complexity and volume of quantum states, which depend on the chosen metric [65, 66]. In particular, the non-uniqueness of these distinguishability measures requires a comprehensive understanding of the physical implications tied to the selection of a specific metric, a subject of considerable conceptual and practical importance [67–70]. Since these complexities surpass the boundaries of our current study, we intend to tackle certain aspects of these challenges in our future research efforts. In addition, we can expand our comparative analysis to incorporate nonstationary Hamiltonian evolutions defined by significant time-dependent magnetic field configurations [59–63]. Moreover, we emphasize that our analysis is limited to a two-state system, which currently hinders our ability to investigate the connection between our complexity measure and quantum entanglement. However, as a preliminary step towards this objective, we are in the process of extending our methodology to include d -level quantum systems with $d > 2$, within larger finite-dimensional Hilbert spaces [71–79].

Notwithstanding its constraints, we assert that our research signifies a considerable endeavor to forge a link between Krylov's state complexity and our quantum IG measure of complexity. Specifically, it seeks to geometrically interpret Krylov's state complexity by investigating the relationships among the notions of *length* (i.e., a metric of the distance a state has traversed), *spread* (i.e., a metric of the number of independent directions occupied by the state), and *volume* (i.e., a metric of the extent of the multi-dimensional region explored).

Acknowledgments

C.C. (Principal Investigator) and E.C. (Undergraduate Research Aide) acknowledge the partial funding received from the University at Albany-SUNY through the FRAP-B (Faculty Research Award Programs) grant number 102106. Moreover, V.V.A. (Graduate Research Aide) expresses gratitude to the University at Albany-SUNY for providing a Research Internship opportunity as an international student. Finally, the opinions, findings, conclusions, or recommendations presented in this material are solely those of the author(s) and do not necessarily represent the perspectives of their respective Institutions.

[1] S. Baiguera et al., *Quantum complexity in gravity, quantum field theory, and quantum information science*, Phys. Rep. **1159**, 1 (2026).

[2] D. Felice, C. Cafaro, and S. Mancini, *Information geometric methods for complexity*, Chaos **28**, 032101 (2018).

[3] A. N. Kolmogorov, *Three approaches to the quantitative definition of information*, Int. J. Computer Mathematics **2**, 157 (1968).

[4] J. Rissanen, *Modeling by the shortest data description*, Automatica **14**, 465 (1978).

[5] J. Rissanen, *Stochastic complexity and modeling*, Ann. Stat. **14**, 1080 (1986).

[6] M. A. Nielsen and I. L. Chuang, *Quantum Computation and Quantum Information*, Cambridge University Press (2000).

[7] F. G. S. L. Brandao, W. Chemissany, N. Hunter-Jones, R. Kueng, and J. Preskill, *Models of quantum complexity growth*, PRX Quantum **2**, 030316 (2021).

[8] M. A. Nielsen, *A geometric approach to quantum circuit lower bounds*, Quant. Inf. Comput. **6**, 213 (2006).

[9] M. A. Nielsen, M. R. Dowling, M. Gu, and A. M. Doherty, *Quantum computation as geometry*, Science **311**, 1133 (2006).

[10] M. R. Dowling and M. A. Nielsen, *The geometry of quantum computation*, Quant. Inf. Comput. **8**, 861 (2008).

[11] V. Balasubramanian, P. Caputa, J. M. Magan, and O. Wu, *Quantum chaos and the complexity of spread of states*, Phys. Rev. **D106**, 046007 (2022).

[12] D. E. Parker, X. Cao, A. Avdoshkin, T. Scaffidi, and E. Altman, *A universal operator growth hypothesis*, Phys. Rev. **X9**, 041017 (2019).

[13] M. Alishahiha and S. Banerjee, *A universal approach to Krylov state and operator complexities*, SciPost Phys. **15**, 080 (2023).

[14] P. Caputa, J. M. Magan, and D. Patramanis, *Geometry of Krylov complexity*, Phys. Rev. Research **4**, 013041 (2022).

[15] P. Caputa and S. Datta, *Operator growth in 2d CFT*, J. High Energ. Phys. **2021**, 188 (2021).

[16] B. Craps, O. Evnin, and G. Pascuzzi, *A relation between Krylov and Nielsen complexity*, Phys. Rev. Lett. **132**, 160402 (2024).

[17] S. E. Aguilar-Gutierrez and A. Rolph, *Krylov complexity is not a measure of distance between states or operators*, Phys. Rev. **D109**, L081701 (2024).

[18] S. Seetharaman, C. Singh, and R. Nath, *Properties of Krylov state complexity in qubit dynamics*, Phys. Rev. **D111**, 076014 (2025).

[19] C. Cafaro, L. Rossetti, and P. M. Alsing, *Complexity of quantum-mechanical evolutions from probability amplitudes*, Nuclear Physics **B1010**, 116755 (2025).

[20] C. Cafaro, E. Clements, and A. Alanazi, *Aspects of complexity in quantum evolutions on the Bloch sphere*, Eur. Phys. J. Plus **140**, 349 (2025).

[21] J. Anandan and Y. Aharonov, *Geometry of quantum evolution*, Phys. Rev. Lett. **65**, 1697 (1990).

[22] R. Uzdin, U. Günther, S. Rahav, and N. Moiseyev, *Time-dependent Hamiltonians with 100% evolution speed efficiency*, J. Phys. A: Math. Theor. **45**, 415304 (2012).

[23] R. Dandoloff, R. Balakrishnan, and A. R. Bishop, *Two-level systems: Space curve formalism, Berry's phase and Gauss-Bonnet theorem*, J. Phys. A: Math. Gen. **25**, L1105 (1992).

[24] L. Carmel and A. Mann, *Geometrical approach to two-level Hamiltonians*, Phys. Rev. **A61**, 052113 (2000).

[25] R. Balakrishnan and R. Dandoloff, *Classical analogues of the Schrödinger and Heisenberg pictures in quantum mechanics using the Frenet frame of a space curve: An example*, Eur. J. Phys. **25**, 447 (2004).

[26] H. P. Laba and V. M. Tkachuk, *Geometric characteristics of quantum evolution: Curvature and torsion*, Condensed Matter Physics **20**, 13003 (2017).

[27] P. M. Alsing and C. Cafaro, *From the classical Frenet-Serret apparatus to the curvature and torsion of quantum-mechanical evolutions. Part I. Stationary Hamiltonians*, Int. J. Geom. Methods Mod. Phys. **21**, 2450152 (2024).

[28] P. M. Alsing and C. Cafaro, *From the classical Frenet-Serret apparatus to the curvature and torsion of quantum-mechanical evolutions. Part II. Nonstationary Hamiltonians*, Int. J. Geom. Methods Mod. Phys. **21**, 2450151 (2024).

[29] L. Rossetti, C. Cafaro, and P. M. Alsing, *Deviations from geodesic evolutions and energy waste on the Bloch sphere*, Phys. Rev. **A111**, 022441 (2025).

[30] C. Cafaro, L. Rossetti, and P. M. Alsing, *Curvature of quantum evolutions for qubits in time-dependent magnetic fields*, Phys. Rev. **A111**, 012408 (2025).

[31] C. Cafaro and S. A. Ali, *Jacobi fields on statistical manifolds of negative curvature*, Physica **D234**, 70 (2007).

[32] C. Cafaro, *The Information Geometry of Chaos*, Ph. D. Thesis, University at Albany-SUNY, USA (2008).

[33] S. A. Ali and C. Cafaro, *Theoretical investigations of an information geometric approach to complexity*, Rev. Math. Phys. **29**, 1730002 (2017).

[34] D. Felice, C. Cafaro, and S. Mancini, *Information geometric methods for complexity*, Chaos **28**, 032101 (2018).

[35] F. J. Dyson, *The S matrix in quantum electrodynamics*, Phys. Rev. **75**, 1736 (1949).

[36] J. J. Sakurai and J. Napolitano, *Modern Quantum Mechanics*, Cambridge University Press (2020).

[37] L. Allen and J. H. Eberly, *Optical Resonance and Two-Level Atoms*, Dover Publications, Inc. New York (1987).

[38] S. L. Braunstein and C. M. Caves, *Statistical distance and the geometry of quantum states*, Phys. Rev. Lett. **72**, 3439 (1994).

[39] C. Cafaro and S. Mancini, *On Grover's search algorithm from a quantum information geometry viewpoint*, Physica **A391**, 1610 (2012).

[40] C. Cafaro and P. M. Alsing, *Decrease of Fisher information and the information geometry of evolution equations for quantum mechanical probability amplitudes*, Phys. Rev. **E97**, 042110 (2018).

[41] C. Lanczos, *An iteration method for the solution of the eigenvalue problem of linear differential and integral operators*, Journal of Research of the Naval Bureau of Standards **45**, 255 (1950).

[42] G. Floquet, *Sur les équations différentielles linéaires à coefficients périodiques*, Annales Scientifiques de l'École Normale Supérieure **12**, 47 (1883).

[43] J. H. Shirley, *Solution of the Schrödinger equation with a Hamiltonian periodic in time*, Phys. Rev. **138**, 980 (1965).

[44] W. E. Arnoldi, *The principle of minimized iterations in the solution of the matrix eigenvalue problem*, Quarterly of Applied Mathematics **9**, 17 (1951).

[45] A. A. Nizami and A. W. Shrestha, *Krylov construction and complexity for driven quantum systems*, Phys. Rev. **E108**, 054222 (2023).

[46] K. Takahashi and A. del Campo, *Krylov subspace methods for quantum dynamics with time-dependent generators*, Phys. Rev. Lett. **134**, 030401 (2025).

[47] P. Caputa, J. M. Magan, D. Patramanis, and E. Tonni, *Krylov complexity of modular Hamiltonian evolution*, Phys. Rev. **D109**, 086004 (2024).

[48] I. S. Gradshteyn and I. M. Ryzhik, *Tables of Integrals, Series, and Products*, Academic Press (2000).

[49] M. Hamermesh, *Group Theory and Its Application to Physical Problems*, Dover Publications (1989).

[50] T. Frankel, *The Geometry of Physics*, Cambridge University Press (2012).

[51] C. Cafaro, S. Ray, and P. M. Alsing, *Optimal-speed unitary quantum time evolutions and propagation of light with maximal degree of coherence*, Phys. Rev. **A105**, 052425 (2022).

[52] I. I. Rabi, *Space quantization in a gyrating magnetic field*, Phys. Rev. **51**, 652 (1937).

[53] I. I. Rabi, N. F. Ramsey, and J. Schwinger, *Use of rotating coordinates in magnetic resonance problems*, Rev. Mod. Phys. **26**, 167 (1954).

[54] R. P. Feynman, F. Vernon, and R. W. Hellwarth, *Geometrical representation of the Schrödinger equation for solving maser problems*, J. Appl. Phys. **28**, 49 (1957).

[55] L. Landau, *A theory of energy transfer. II*, Phys. Z. Sowjet **2**, 46 (1932).

[56] C. Zener, *Non-adiabatic crossing of energy levels*, Proc. R. Soc. **A137**, 696 (1932).

[57] E. Barnes and S. Das Sarma, *Analytically solvable driven time-dependent two-level quantum systems*, Phys. Rev. Lett. **109**, 060401 (2012).

[58] E. Barnes, *Analytically solvable two-level quantum systems and Landau-Zener interferometry*, Phys. Rev. **A88**, 013818 (2013).

[59] A. Messina and H. Nakazato, *Analytically solvable Hamiltonians for quantum two-level systems and their dynamics*, J. Phys. A: Math and Theor. **47**, 44302 (2014).

[60] R. Grimaudo, A. S. Magalhaes de Castro, H. Nakazato, and A. Messina, *Classes of exactly solvable generalized semi-classical Rabi systems*, Annalen der Physik **530**, 1800198 (2018).

[61] C. Cafaro and P. M. Alsing, *Continuous-time quantum search and time-dependent two-level quantum systems*, Int. J. Quantum Information **17**, 1950025 (2019).

[62] L. O. Castanos, *Simple, analytic solutions of the semiclassical Rabi model*, Optics Communications **430**, 176 (2019).

[63] A. S. Magalhaes de Castro, R. Grimaudo, D. Valenti, A. Migliore, H. Nakazato, and A. Messina, *Analytically solvable Hamiltonian in invariant subspaces*, Eur. Phys. J. Plus **138**, 766 (2023).

[64] E. R. Loubenets and C. Kading, *Specifying the unitary evolution of a qudit for a general nonstationary Hamiltonian via the generalized Gell-Mann representation*, Entropy **22**, 521 (2020).

[65] C. Cafaro and P. M. Alsing, *Bures and Sjöqvist metrics over thermal state manifolds for spin qubits and superconducting flux qubits*, Eur. Phys. J. Plus **138**, 655 (2023).

[66] P. M. Alsing, C. Cafaro, O. Luongo, C. Lupo, S. Mancini, and H. Quevedo, *Comparing metrics for mixed quantum states: Sjöqvist and Bures*, Phys. Rev. A **107**, 052411 (2023).

[67] H. Silva, B. Mera, and N. Paunkovic, *Interferometric geometry from symmetry-broken Uhlmann gauge group with applications to topological phase transitions*, Phys. Rev. B **103**, 085127 (2021).

[68] B. Mera, N. Paunkovic, S. T. Amin, and V. R. Vieira, *Information geometry of quantum critical submanifolds: Relevant, marginal, and irrelevant operators*, Phys. Rev. B **106**, 155101 (2022).

[69] P. M. Alsing, C. Cafaro, D. Felice, and O. Luongo, *Geometric aspects of mixed quantum states inside the Bloch sphere*, Quantum Reports **6**, 90 (2024).

[70] X.-Y. Hou, Z. Zhou, X. Wang, H. Guo, and C.-C. Chien, *Local geometry and quantum geometric tensor of mixed states*, Phys. Rev. B **110**, 035144 (2024).

[71] L. Jakobczyk and M. Siennicki, *Geometry of Bloch vectors in two-qubit system*, Phys. Lett. A **286**, 383 (2001).

[72] G. Kimura, *The Bloch vector for N-level systems*, Phys. Lett. A **314**, 339 (2003).

[73] R. A. Bertlmann and P. Krammer, *Bloch vectors for qudits*, J. Phys. A: Math. Theor. **41**, 235303 (2008).

[74] P. Kurzynski, *Multi-Bloch vector representation of the qutrit*, Quantum Inf. Comp. **11**, 361 (2011).

[75] J. Xie et al., *Observing geometry of quantum states in a three-level system*, Phys. Rev. Lett. **125**, 150401 (2020).

[76] C. Eltschka, M. Huber, S. Morelli, and J. Siewert, *The shape of higher-dimensional state space: Bloch-ball analog for a qutrit*, Quantum **5**, 485 (2021).

[77] G. Sharma, S. Ghosh, and Sk Sazim, *Bloch sphere analog of qudits using Heisenberg-Weyl operators*, Phys. Scr. **99**, 045105 (2024).

[78] S. Morelli, C. Eltschka, M. Huber, and J. Siewert, *Correlation constraints and the Bloch geometry of two qubits*, Phys. Rev. A **109**, 012423 (2024).

[79] S. Sen and T. K. Dey, *Phase portrait of the qutrit system*, Phys. Scr. **100**, 095104 (2025).

[80] J. P. Provost and G. Vallee, *Riemannian structure on manifolds of quantum states*, Commun. Math. Phys. **76**, 289 (1980).

[81] S. Luo, *Wigner-Yanase skew information and uncertainty relations*, Phys. Rev. Lett. **91**, 180403 (2003).

[82] S. Luo, *Fisher information of wavefunctions: Classical and quantum*, Chin. Phys. Lett. **23**, 3127 (2006).

[83] I. Bengtsson and K. Zyczkowski, *Geometry of Quantum States*, Cambridge University Press (2006).

[84] S. Amari and H. Nagaoka, *Methods of Information Geometry*, Cambridge University Press (2000).

[85] K. M. Lynch and F. C. Park, *Modern Robotics: Mechanics, Planning, and Control*, Cambridge University Press (2017).

Appendix A: Relation between Fubini-Study and Wigner-Yanase metrics

In this appendix, we show that the Fubini-Study metric g_{FS} is proportional to the quantum Fisher information metric g_{QFI} (with $g_{\text{QFI}} = 4g_{\text{FS}}$). Indeed, the geometry of the Bloch sphere, when utilizing the Fubini-Study metric [80], can be viewed as a quantum information geometric framework for pure quantum states that are associated with the Wigner-Yanase metric [81, 82]. The Wigner-Yanase metric serves as a quantum information-geometric metric that is defined within the realm of quantum states [83]. In the case of diagonal density matrices, the Wigner-Yanase metric simplifies to the classical Fisher-Rao information metric [84]. Conversely, for pure states, the Wigner-Yanase metric aligns (up to a multiplicative factor) with the Fubini-Study metric. In this appendix, we will illustrate this assertion.

1. Fubini-Study metric

We begin by presenting the Fubini-Study metric tensor components $g_{ab}^{\text{FS}}(\xi)$. We will consider a collection of quantum state vectors $\{|\psi(\xi)\rangle\}$ that are parameterized by the parameters $\xi \stackrel{\text{def}}{=} (\xi^1, \dots, \xi^m)$. Here, m represents the number of real-valued parameters that are assumed to characterize a quantum state $|\psi(\xi)\rangle$ in $\mathbb{C}P^{n-1}$. For the sake of clarity, we will assume that \mathcal{H} is the n -dimensional complex Hilbert space \mathcal{H}_2^N of N -qubit quantum states with $n = 2^N$, and we concentrate on the straightforward case where $n = 2$. Consequently, irrespective of the selected definition of finite distance, the infinitesimal line element ds_{FS}^2 which measures the distance between two neighboring states $|\psi(\xi)\rangle$ and $|\psi(\xi + d\xi)\rangle$ can be expressed as

$$ds_{\text{FS}}^2 = g_{ab}(\xi) d\xi^a d\xi^b. \quad (\text{A1})$$

The metric tensor components $g_{ab}(\xi)$ in Eq. (A1) are given by [80],

$$g_{ab}(\xi) \stackrel{\text{def}}{=} [\gamma_{ab}(\xi) - \beta_a(\xi) \beta_b(\xi)], \quad (\text{A2})$$

where, assuming $\partial_a \stackrel{\text{def}}{=} \partial/\partial\xi^a$, we define

$$\gamma_{ab}(\xi) \stackrel{\text{def}}{=} \text{Re}[\langle \partial_a \psi(\xi) | \partial_b \psi(\xi) \rangle], \text{ and } \beta_a(\xi) \stackrel{\text{def}}{=} -i \langle \psi(\xi) | \partial_a \psi(\xi) \rangle. \quad (\text{A3})$$

From Eq. (A3), we observe that

$$\beta_a(\xi) \beta_b(\xi) = \langle \partial_a \psi(\xi) | \psi(\xi) \rangle \langle \psi(\xi) | \partial_b \psi(\xi) \rangle, \quad (\text{A4})$$

given that $\partial_a [\langle \psi(\xi) | \psi(\xi) \rangle] = 0$ leads to $\langle \psi(\xi) | \partial_a \psi(\xi) \rangle = -\langle \partial_a \psi(\xi) | \psi(\xi) \rangle$. Therefore, making use of Eqs. (A3) and (A4), $g_{ab}(\xi)$ in Eq. (A2) reduces to

$$g_{ab}(\xi) = \{\text{Re}[\langle \partial_a \psi(\xi) | \partial_b \psi(\xi) \rangle] - \langle \partial_a \psi(\xi) | \psi(\xi) \rangle \langle \psi(\xi) | \partial_b \psi(\xi) \rangle\}. \quad (\text{A5})$$

For simplicity, let us introduce

$$A_{ab}(\xi) \stackrel{\text{def}}{=} \langle \partial_a \psi(\xi) | \psi(\xi) \rangle \langle \psi(\xi) | \partial_b \psi(\xi) \rangle. \quad (\text{A6})$$

We shall verify that $A_{ab}(\xi) d\xi^a d\xi^b = \text{Re}[A_{ab}(\xi)] d\xi^a d\xi^b$. Take into consideration,

$$A_{ab}(\xi) = \text{Re}[A_{ab}(\xi)] + i \text{Im}[A_{ab}(\xi)] = A_{ab}^{(1)}(\xi) + i A_{ab}^{(2)}(\xi). \quad (\text{A7})$$

Then, from Eq. (A6), we arrive at

$$\begin{aligned} A_{ab}^{(1)}(\xi) &= \text{Re}[A_{ab}(\xi)] \\ &= \text{Re}[\langle \partial_a \psi(\xi) | \psi(\xi) \rangle \langle \psi(\xi) | \partial_b \psi(\xi) \rangle] \\ &= \text{Re}[\langle \partial_a \psi(\xi) | \psi(\xi) \rangle^* \langle \psi(\xi) | \partial_b \psi(\xi) \rangle^*] \\ &= \text{Re}[\langle \psi(\xi) | \partial_a \psi(\xi) \rangle \langle \partial_b \psi(\xi) | \psi(\xi) \rangle] \\ &= \text{Re}[\langle \partial_b \psi(\xi) | \psi(\xi) \rangle \langle \psi(\xi) | \partial_a \psi(\xi) \rangle] \\ &= \text{Re}[A_{ba}(\xi)] \\ &= A_{ba}^{(1)}(\xi), \end{aligned} \quad (\text{A8})$$

and, moreover,

$$\begin{aligned}
A_{ab}^{(2)}(\xi) &= \text{Im}[A_{ab}(\xi)] \\
&= \text{Im}[\langle \partial_a \psi(\xi) | \psi(\xi) \rangle \langle \psi(\xi) | \partial_b \psi(\xi) \rangle] \\
&= -\text{Im}[\langle \partial_a \psi(\xi) | \psi(\xi) \rangle^* \langle \psi(\xi) | \partial_b \psi(\xi) \rangle^*] \\
&= -\text{Im}[\langle \partial_b \psi(\xi) | \psi(\xi) \rangle \langle \psi(\xi) | \partial_a \psi(\xi) \rangle] \\
&= -\text{Im}[A_{ba}(\xi)] \\
&= -A_{ba}^{(2)}(\xi).
\end{aligned} \tag{A9}$$

Eqs. (A8) and (A9) imply that $A_{ab}^{(1)}(\xi)$ is symmetric under exchange of indices, whereas $A_{ab}^{(2)}(\xi)$ is antisymmetric. Therefore, given the symmetry of $d\xi^a d\xi^b$, we obtain $A_{ab}(\xi) d\xi^a d\xi^b = \text{Re}[A_{ab}(\xi)] d\xi^a d\xi^b$. Summing up, $g_{ab}(\xi)$ can be recast as

$$g_{ab}(\xi) = \text{Re}[\langle \partial_a \psi(\xi) | \partial_b \psi(\xi) \rangle] - \text{Re}[\langle \partial_a \psi(\xi) | \psi(\xi) \rangle \langle \psi(\xi) | \partial_b \psi(\xi) \rangle], \tag{A10}$$

that is,

$$g_{ab}^{\text{FS}}(\xi) = \text{Re}[\langle \partial_a \psi(\xi) | \partial_b \psi(\xi) \rangle - \langle \partial_a \psi(\xi) | \psi(\xi) \rangle \langle \psi(\xi) | \partial_b \psi(\xi) \rangle]. \tag{A11}$$

Eq. (A11) specifies the Fubini-Study metric tensor on the manifold of pure quantum states.

2. Wigner-Yanase metric

We now present the Wigner-Yanase metric tensor components $g_{ab}^{\text{WY}}(\xi)$. We begin by recalling that the so-called Wigner-Yanase metric $g_{ab}^{\text{WY}}(\xi)$ is defined as [81, 82],

$$g_{ab}^{\text{WY}}(\xi) \stackrel{\text{def}}{=} 4\text{tr}[(\partial_a \sqrt{\rho_\xi}) (\partial_b \sqrt{\rho_\xi})] = 4\text{tr}[(\partial_a \rho_\xi) (\partial_b \rho_\xi)], \tag{A12}$$

since $\rho_\xi = \rho_\xi^2$ with $\rho_\xi \stackrel{\text{def}}{=} |\psi(\xi)\rangle \langle \psi(\xi)| = |\psi_\xi\rangle \langle \psi_\xi|$ denoting a pure state. Note that $\partial_a \rho_\xi$ in Eq. (A12) can be recast as,

$$\partial_a \rho_\xi = \partial_a (|\psi_\xi\rangle \langle \psi_\xi|) = |\partial_a \psi_\xi\rangle \langle \psi_\xi| + |\psi_\xi\rangle \langle \partial_a \psi_\xi|. \tag{A13}$$

Therefore, after some simple algebraic manipulations, we arrive at

$$\begin{aligned}
(\partial_a \rho_\xi) (\partial_b \rho_\xi) &= \langle \psi_\xi | \partial_b \psi_\xi \rangle \langle \partial_a \psi_\xi \rangle \langle \psi_\xi | + |\partial_a \psi_\xi\rangle \langle \partial_b \psi_\xi| + \langle \partial_a \psi_\xi | \partial_b \psi_\xi \rangle |\psi_\xi\rangle \langle \psi_\xi| + \\
&\quad + \langle \partial_a \psi_\xi | \psi_\xi \rangle |\psi_\xi\rangle \langle \partial_b \psi_\xi|.
\end{aligned} \tag{A14}$$

Employing Eq. (A14), $\text{tr}[(\partial_a \rho_\xi) (\partial_b \rho_\xi)]$ in Eq. (A12) can be rewritten as

$$\begin{aligned}
\text{tr}[(\partial_a \rho_\xi) (\partial_b \rho_\xi)] &= \langle \psi_\xi | (\partial_a \rho_\xi) (\partial_b \rho_\xi) | \psi_\xi \rangle \\
&= \langle \psi_\xi | \partial_b \psi_\xi \rangle \langle \psi_\xi | \partial_a \psi_\xi \rangle + \langle \psi_\xi | \partial_a \psi_\xi \rangle \langle \partial_b \psi_\xi | \psi_\xi \rangle + \\
&\quad + \langle \partial_a \psi_\xi | \partial_b \psi_\xi \rangle + \langle \partial_a \psi_\xi | \psi_\xi \rangle \langle \partial_b \psi_\xi | \psi_\xi \rangle.
\end{aligned} \tag{A15}$$

We observe that the normalization condition $\langle \psi_\xi | \psi_\xi \rangle = 1$ implies that $\langle \partial_b \psi_\xi | \psi_\xi \rangle = -\langle \psi_\xi | \partial_b \psi_\xi \rangle$. Therefore, $\text{tr}[(\partial_a \rho_\xi) (\partial_b \rho_\xi)]$ in Eq. (A15) reduces to

$$\text{tr}[(\partial_a \rho_\xi) (\partial_b \rho_\xi)] = \langle \partial_a \psi_\xi | \partial_b \psi_\xi \rangle + \langle \partial_a \psi_\xi | \psi_\xi \rangle \langle \partial_b \psi_\xi | \psi_\xi \rangle. \tag{A16}$$

Following Ref. [80], the inner product $\langle \partial_a \psi_\theta | \partial_b \psi_\theta \rangle$ can be recast as

$$\langle \partial_a \psi_\xi | \partial_b \psi_\xi \rangle = \gamma_{ab} + i\sigma_{ab}, \tag{A17}$$

where γ_{ab} and σ_{ab} are defined as

$$\gamma_{ab} \stackrel{\text{def}}{=} \text{Re} [\langle \partial_a \psi_\xi | \partial_b \psi_\xi \rangle], \text{ and } \sigma_{ab} \stackrel{\text{def}}{=} \text{Im} [\langle \partial_a \psi_\xi | \partial_b \psi_\xi \rangle], \quad (\text{A18})$$

respectively. Observe that $\text{Re}(z)$ and $\text{Im}(z)$ represent the real and imaginary parts of a complex quantity z , respectively. Note that γ_{ab} and σ_{ab} in Eq. (A18) are symmetric and antisymmetric quantities, respectively. Indeed, we have

$$\gamma_{ba} = \text{Re} [\langle \partial_b \psi_\xi | \partial_a \psi_\xi \rangle] = \text{Re} [\langle \partial_a \psi_\xi | \partial_b \psi_\xi \rangle^*] = \text{Re} [\langle \partial_a \psi_\xi | \partial_b \psi_\xi \rangle] = \gamma_{ab}, \quad (\text{A19})$$

and,

$$\sigma_{ba} = \text{Im} [\langle \partial_b \psi_\xi | \partial_a \psi_\xi \rangle] = \text{Im} [\langle \partial_a \psi_\xi | \partial_b \psi_\xi \rangle^*] = -\text{Im} [\langle \partial_a \psi_\xi | \partial_b \psi_\xi \rangle] = -\sigma_{ab}. \quad (\text{A20})$$

Since $\sigma_{ab} = -\sigma_{ba}$, $\sigma_{ab} d\xi^a d\xi^b = 0$. By using Eqs. (A16), (A17) and (A18), $g_{ab}^{\text{WY}}(\xi)$ in Eq. (A12) becomes

$$g_{ab}^{\text{WY}}(\xi) = 4 \text{Re} [\langle \partial_a \psi_\xi | \partial_b \psi_\xi \rangle - \langle \partial_a \psi_\xi | \psi_\xi \rangle \langle \psi_\xi | \partial_b \psi_\xi \rangle], \quad (\text{A21})$$

since $\langle \partial_a \psi_\xi | \psi_\xi \rangle \langle \psi_\xi | \partial_b \psi_\xi \rangle$ is a real-valued quantity. Comparing Eqs. (A11) and (A21), we finally arrive at the relation $g_{ab}^{\text{WY}}(\xi) = 4g_{ab}^{\text{FS}}(\xi)$. For further details, we suggest Refs. [39, 40]. With this statement, we conclude our discussion on the link between Fubini-Study and Wigner-Yanase metrics at this point.

Appendix B: Rotation matrix $\mathcal{R}(t)$

In this appendix, we find the explicit expression of the rotation matrix $\mathcal{R}(t)$ such that $\mathbf{a}(t) = \mathcal{R}(t)\mathbf{a}(0)$, when $\dot{\mathbf{a}} = (2/\hbar)\mathbf{h} \times \mathbf{a}$, the Hamiltonian $H \stackrel{\text{def}}{=} \mathbf{h} \cdot \boldsymbol{\sigma}$ is time-independent, and $\mathbf{h} \stackrel{\text{def}}{=} h\mathbf{n}$ with $h \stackrel{\text{def}}{=} \|\mathbf{h}\|$.

We start by noting that the equation $\dot{\mathbf{a}} = (2/\hbar)\mathbf{h} \times \mathbf{a}$ can be recast as $\dot{\mathbf{a}} = (2/\hbar)H_{\mathbf{h}}\mathbf{a}$, with $H_{\mathbf{h}}$ being a (3×3) -matrix defined as

$$H_{\mathbf{h}} \stackrel{\text{def}}{=} \begin{pmatrix} 0 & -h_z & h_y \\ h_z & 0 & -h_x \\ -h_y & h_x & 0 \end{pmatrix}. \quad (\text{B1})$$

Therefore, after a brief inspection, one realizes that integration of $\dot{\mathbf{a}} = (2/\hbar)H_{\mathbf{h}}\mathbf{a}$ yields

$$\mathbf{a}(t) = e^{\frac{2}{\hbar}H_{\mathbf{h}}t}\mathbf{a}(0), \quad (\text{B2})$$

with $\mathcal{R}(t) = e^{\frac{2}{\hbar}H_{\mathbf{h}}t} = e^{\frac{2h}{\hbar}\frac{H_{\mathbf{h}}}{h}t} = e^{\frac{2h}{\hbar}H_{\mathbf{n}}t} = \mathcal{R}_{\mathbf{n}}(\frac{2h}{\hbar}t)$ being a rotation with axis of rotation \mathbf{n} and angle of rotation $\frac{2h}{\hbar}t$. Recalling the Rodrigues rotation formula in matrix form [85], we observe that $\mathcal{R}_{\mathbf{n}}(\frac{2h}{\hbar}t)$ can be rewritten as

$$\mathcal{R}_{\mathbf{n}}\left(\frac{2h}{\hbar}t\right) = \cos\left(\frac{2h}{\hbar}t\right)I_{3 \times 3} + \left[1 - \cos\left(\frac{2h}{\hbar}t\right)\right](\mathbf{n} \cdot \mathbf{n}^T) + \sin\left(\frac{2h}{\hbar}t\right)H_{\mathbf{n}}, \quad (\text{B3})$$

where $I_{3 \times 3}$ is the (3×3) -identity matrix, $(\mathbf{n} \cdot \mathbf{n}^T)$ is the (3×3) -matrix obtained from the matrix algebra multiplication between the column vector \mathbf{n} and the row vector \mathbf{n}^T (with “ T ” denoting the transposition operation), and $H_{\mathbf{n}} \stackrel{\text{def}}{=} (1/h)H_{\mathbf{h}}$ with $H_{\mathbf{h}}$ in Eq. (B1). We can explicitly verify from Eq. (B3) that $\mathcal{R}_{\mathbf{n}}(0) = I_{3 \times 3}$ and $\mathcal{R}_{\mathbf{n}}(\frac{2h}{\hbar}t) \in \text{SO}(3; \mathbb{R})$ with $\det[\mathcal{R}_{\mathbf{n}}(\frac{2h}{\hbar}t)] = 1$. From Eq. (B3), we notice that $\mathbf{a}_t = \mathcal{R}_{\mathbf{n}}(\frac{2h}{\hbar}t)\mathbf{a}_0$ reduces to

$$\mathbf{a}_t = \cos\left(\frac{2h}{\hbar}t\right)\mathbf{a}_0 + \left[1 - \cos\left(\frac{2h}{\hbar}t\right)\right](\mathbf{n} \cdot \mathbf{a}_0)\mathbf{n} + \sin\left(\frac{2h}{\hbar}t\right)(\mathbf{n} \times \mathbf{a}_0), \quad (\text{B4})$$

since $(\mathbf{n} \cdot \mathbf{n}^T)\mathbf{a}_0 = (\mathbf{n} \cdot \mathbf{a}_0)\mathbf{n}$ is the projection of \mathbf{a}_0 onto \mathbf{n} and $H_{\mathbf{n}}\mathbf{a}_0 = \mathbf{n} \times \mathbf{a}_0$. Clearly, \mathbf{a}_t and \mathbf{a}_0 denote $\mathbf{a}(t)$ and $\mathbf{a}(0)$, respectively. To understand Eq. (B4), one can decompose \mathbf{a}_0 relative to the rotation axis \mathbf{n} as $\mathbf{a}_0^{\parallel} = (\mathbf{n} \cdot \mathbf{a}_0)\mathbf{n}$ (i.e., a part parallel to \mathbf{n}) and $\mathbf{a}_0^{\perp} = \mathbf{a}_0 - \mathbf{a}_0^{\parallel}$ (i.e., a part orthogonal to \mathbf{n}). Since \mathbf{a}_0^{\parallel} lies along the axis \mathbf{n} , it does

not change under rotation and $\mathbf{a}_0^{\parallel}(t) = \mathbf{a}_0^{\parallel}(0)$. The orthogonal component \mathbf{a}_0^{\perp} rotates in the plane orthogonal to \mathbf{n} , $\mathbf{a}_0^{\perp}(t) = \cos(\frac{2h}{\hbar}t)\mathbf{a}_0^{\perp}(0) + \sin(\frac{2h}{\hbar}t)\mathbf{n} \times \mathbf{a}_0^{\perp}(0)$. Therefore, we have

$$\begin{aligned}\mathbf{a}(t) &= \mathbf{a}_0^{\parallel}(0) + \mathbf{a}_0^{\perp}(0) \\ &= \mathbf{a}_0^{\parallel}(0) + \cos(\frac{2h}{\hbar}t)\mathbf{a}_0^{\perp}(0) + \sin(\frac{2h}{\hbar}t)[\mathbf{n} \times \mathbf{a}_0^{\perp}(0)] \\ &= (\mathbf{n} \cdot \mathbf{a}_0)\mathbf{n} + \cos(\frac{2h}{\hbar}t)[\mathbf{a}_0 - (\mathbf{n} \cdot \mathbf{a}_0)\mathbf{n}] + \sin(\frac{2h}{\hbar}t)(\mathbf{n} \times \mathbf{a}_0) \\ &= \cos(\frac{2h}{\hbar}t)\mathbf{a}_0 + \left[1 - \cos(\frac{2h}{\hbar}t)\right](\mathbf{n} \cdot \mathbf{a}_0)\mathbf{n} + \sin(\frac{2h}{\hbar}t)(\mathbf{n} \times \mathbf{a}_0),\end{aligned}\quad (B5)$$

where in the second to last line we used the fact that $\mathbf{n} \times \mathbf{a}_0^{\perp}(0) = \mathbf{n} \times \mathbf{a}_0$. Clearly, since $\mathbf{a}_t = \mathbf{a}(t)$, Eqs. (B4) and (B5) are identical. Finally, given that the vector triple product $\mathbf{n} \times (\mathbf{n} \times \mathbf{a}_0)$ is equal to $(\mathbf{n} \cdot \mathbf{a}_0)\mathbf{n} - (\mathbf{n} \cdot \mathbf{n})\mathbf{a}_0 = (\mathbf{n} \cdot \mathbf{a}_0)\mathbf{n} - \mathbf{a}_0$, Eq. (B4) can be recast as

$$\mathbf{a}_t = \mathbf{a}_0 + \sin\left(\frac{2h}{\hbar}t\right)(\mathbf{n} \times \mathbf{a}_0) + \left[1 - \cos\left(\frac{2h}{\hbar}t\right)\right][\mathbf{n} \times (\mathbf{n} \times \mathbf{a}_0)].\quad (B6)$$

Eq. (B6) is the vectorial form of the so-called Rodrigues rotation formula [85].

For completeness, we stress that the interested reader can verify that Eq. (B3) works properly. For example, one can recover \mathbf{a}_t in Eq. (61) as $\mathbf{a}_t = \mathcal{R}_{\mathbf{n}}(\frac{2h}{\hbar}t)\mathbf{a}_0$ by setting $\mathbf{a}_0 = (0, 0, 1)$, $\mathbf{n} = (0, 1, 0)$, and $h = \|\mathbf{h}\| = (\hbar\omega)/\sqrt{6}$. Indeed, a simple calculation yields

$$\mathbf{a}_t = \mathcal{R}_{\mathbf{n}}(\frac{2h}{\hbar}t)\mathbf{a}_0 = \begin{pmatrix} \cos(\frac{2\omega t}{\sqrt{6}}) & 0 & \sin(\frac{2\omega t}{\sqrt{6}}) \\ 0 & 1 & 0 \\ -\sin(\frac{2\omega t}{\sqrt{6}}) & 0 & \cos(\frac{2\omega t}{\sqrt{6}}) \end{pmatrix} \begin{pmatrix} 0 \\ 0 \\ 1 \end{pmatrix} = \begin{pmatrix} \sin(\frac{2\omega t}{\sqrt{6}}) \\ 0 \\ \cos(\frac{2\omega t}{\sqrt{6}}) \end{pmatrix}.\quad (B7)$$

Following this verification, we conclude our discussion on the rotation matrix $\mathcal{R}(t)$ at this point.

Appendix C: Basis independence of quantum IG complexity

In this appendix, we discuss the fact that our complexity measure C does not depend on the orthonormal basis chosen to express the time-evolved quantum state of the system. However, although \bar{V} and V_{\max} do not change, the temporal dependence of the instantaneous volume $V(t)$ can depend on the particular basis chosen.

For clarity of exposition, assume the evolution from $\frac{|0\rangle+i|1\rangle}{\sqrt{2}}$ to $|0\rangle$ under $H = \mathbb{E}\sigma_x$. With respect to the computational basis $\{|0\rangle, |1\rangle\}$ and the eigenbasis $\{|E_0\rangle \stackrel{\text{def}}{=} \frac{|0\rangle+i|1\rangle}{\sqrt{2}}, |E_1\rangle \stackrel{\text{def}}{=} \frac{|0\rangle-i|1\rangle}{\sqrt{2}}\}$ (which, in this particular case, coincides with the Krylov basis $\{|K_0\rangle = |E_0\rangle, |K_1\rangle = |E_1\rangle\}$), the time-evolved state $|\psi(t)\rangle$ is given by

$$|\psi(t)\rangle = \frac{\cos(\frac{E}{\hbar}t) + \sin(\frac{E}{\hbar}t)}{\sqrt{2}}|0\rangle + i\frac{\cos(\frac{E}{\hbar}t) - \sin(\frac{E}{\hbar}t)}{\sqrt{2}}|1\rangle,\quad (C1)$$

and,

$$|\psi(t)\rangle = \cos(\frac{E}{\hbar}t)|K_0\rangle + \sin(\frac{E}{\hbar}t)|K_1\rangle,\quad (C2)$$

respectively. The spherical angles that parametrize the qubit in the states in Eqs. (C1) and (C2) are given by

$$\theta(t) = 2 \arctan \left(\sqrt{\left(\frac{\cos(\frac{E}{\hbar}t) - \sin(\frac{E}{\hbar}t)}{\cos(\frac{E}{\hbar}t) + \sin(\frac{E}{\hbar}t)} \right)^2} \right), \varphi(t) = \frac{\pi}{2},\quad (C3)$$

and,

$$\theta(t) = \frac{2E}{\hbar}t, \varphi(t) = 0,\quad (C4)$$

respectively, with $0 \leq t \leq (\pi\hbar)/(4E)$. For completeness, we emphasize that although we use the same notation for the spherical angles in Eqs. (C3) and (C4), the z -axis is specified by the state $|0\rangle$ in Eq. (C3), while $|K_0\rangle$ defines the z -axis in Eq. (C4). Setting $E = 1 = \hbar$ for simplicity, we note that although $V(t)$ for Eq. (C3) differs from $V(t)$ for Eq. (C4), we have

$$\int_0^{\frac{\pi}{4}} t dt = \frac{\pi^2}{32} = \int_0^{\frac{\pi}{4}} \left[\frac{\pi}{4} - \arctan \left(\sqrt{\left(\frac{\cos(\frac{E}{\hbar}t) - \sin(\frac{E}{\hbar}t)}{\cos(\frac{E}{\hbar}t) + \sin(\frac{E}{\hbar}t)} \right)^2} \right) \right] dt. \quad (\text{C5})$$

Therefore, after some inspection, we have $(\bar{V})_{\text{Eq. (C3)}} = \pi/8 = (\bar{V})_{\text{Eq. (C4)}}$ and $(V_{\max})_{\text{Eq. (C3)}} = \pi/4 = (V_{\max})_{\text{Eq. (C4)}}$. Finally, we show that $(C)_{\text{Eq. (C1)}} = (C)_{\text{Eq. (C2)}}$.

Appendix D: Links between $\mathcal{K}(t)$, $\|\mathbf{a}(t) - \mathbf{a}(0)\|^2$, and $V_{\text{FS}}(t)$

In this appendix, to gain some understanding of the connections between Krylov's state complexity $\mathcal{K}(t)$, the distance squared $\|\mathbf{a}(t) - \mathbf{a}(0)\|^2$ between the initial Bloch vector and the Bloch vector at an instant t with $0 \leq t \leq t_f$, and the Fubini-Study volume element $V_{\text{FS}}(t)$, we consider an arbitrary stationary Hamiltonian H with a spectral decomposition given by,

$$H \stackrel{\text{def}}{=} E_0 |E_0\rangle\langle E_0| + E_1 |E_1\rangle\langle E_1|. \quad (\text{D1})$$

Assume the initial state of the system is $|\psi(0)\rangle \stackrel{\text{def}}{=} \cos(\frac{\theta_0}{2}) |E_0\rangle + e^{i\varphi_0} \sin(\frac{\theta_0}{2}) |E_1\rangle$. Then, the time-evolved state $|\psi(t)\rangle \stackrel{\text{def}}{=} e^{-\frac{i}{\hbar}Ht} |\psi(0)\rangle$ is physically equivalent to the state

$$|\psi(t)\rangle \simeq \cos(\frac{\theta_0}{2}) |E_0\rangle + e^{i(\varphi_0 + \Delta Et)} \sin(\frac{\theta_0}{2}) |E_1\rangle, \quad (\text{D2})$$

where $\Delta E \stackrel{\text{def}}{=} E_0 - E_1$, and $H|E_i\rangle = E_i |E_i\rangle$ for $i \in \{0, 1\}$. From Eq. (D2), the time evolution of the spherical angles that parametrize the qubit $|\psi(t)\rangle$ on the Bloch sphere is specified by $\theta(t) = \theta_0$ and $\varphi(t) = \varphi_0 + \Delta Et$. A simple calculation yields

$$\mathcal{K}(t) = \sin^2(\theta_0) \sin^2(\frac{\Delta E}{2}t), \quad \|\mathbf{a}(t) - \mathbf{a}(0)\|^2 = 4\mathcal{K}(t), \quad \text{and} \quad V_{\text{FS}}(t) = \sin(\theta_0) \frac{\Delta E}{2} t. \quad (\text{D3})$$

For completeness, we recall that the Fubini-Study line element is given by $ds_{\text{FS}}^2 \stackrel{\text{def}}{=} \frac{1}{4} [d\theta^2 + \sin^2(\theta) d\varphi^2]$ and, in general, $V_{\text{FS}}(t) = \int dV_{\text{FS}}(t)$ with $dV_{\text{FS}}(t) = \frac{1}{4} \sqrt{\sin^2(\theta)} d\theta d\varphi$. Clearly, when $\theta(t) = \theta_0$ is constant, we have $dV_{\text{FS}}(t) = \frac{1}{2} \sin(\theta_0) d\varphi$. Moreover, the Krylov basis used to calculate $\mathcal{K}(t)$ in Eq. (D3) is given by $\{|K_0\rangle, |K_1\rangle\}$ where $|K_0\rangle = |\psi(0)\rangle \stackrel{\text{def}}{=} |\psi_0(\theta_0, \varphi_0)\rangle$ and $|K_1\rangle \stackrel{\text{def}}{=} |\psi_0(\pi - \theta_0, \pi + \varphi_0)\rangle = \sin(\frac{\theta_0}{2}) |E_0\rangle - e^{i\varphi_0} \cos(\frac{\theta_0}{2}) |E_1\rangle$. From Eq. (D3), we observe that

$$\mathcal{K}(t) = \frac{1}{4} \|\mathbf{a}(t) - \mathbf{a}(0)\|^2, \quad \text{and} \quad \sqrt{\mathcal{K}(t)} \stackrel{t \ll 1}{\approx} V_{\text{FS}}(t). \quad (\text{D4})$$

Eq. (D4) implies that Krylov's state complexity $\mathcal{K}(t)$ in qubit dynamics is proportional to the Euclidean distance between the initial and the final (i.e., at time t) Bloch vectors that specify the qubit on the Bloch sphere. Moreover, Eq. (D4) leads to the conclusion that the square root of Krylov's state complexity $\mathcal{K}(t)$ is approximately equal to the instantaneous volume $V_{\text{FS}}(t)$ in the short-time limit. It is noteworthy to mention that for short times, $V_{\text{FS}}(t)$ (which, in this instance, represents the Fubini-Study length) increases linearly, whereas Krylov's state complexity escalates quadratically. The emergence of the quadratic behavior is universal and signifies that the probability flow into new Krylov levels is second order in time. This universality arises from the unitarity of quantum-mechanical time evolution, the Taylor expansion of $e^{-\frac{i}{\hbar}Ht}$, and the Born rule (i.e., probability = $|\text{amplitude}|^2$). The flow of probability is characterized as second order in time. If $|K_0\rangle \stackrel{\text{def}}{=} |\psi_0\rangle$ represents the initial Krylov state, the time-evolved state can be expressed as

$$|\psi(t)\rangle = e^{-\frac{i}{\hbar}Ht} |\psi_0\rangle = \left[\mathbf{1} - i \frac{H}{\hbar} t - \frac{1}{2} \frac{H^2}{\hbar^2} t^2 + \mathcal{O}(t^3) \right] |\psi_0\rangle, \quad (\text{D5})$$

it follows that the amplitude for transitioning from $|K_0\rangle$ is linear in t , specifically $\langle K_1 | \psi(t) \rangle \sim -\frac{i}{\hbar} \langle K_1 | H | K_0 \rangle t$. Consequently, the probability of transitioning to a new Krylov level is second order in time, as indicated by $|\langle K_1 | \psi(t) \rangle|^2 \sim t^2$. With these considerations, we end our presentation here.